SCALING ANALYSIS OF MELTING KINETICS IN RANDOMLY PACKED STEEL SCRAP IN ELECTRIC ARC FURNACE STEEL MAKING

SCALING ANALYSIS OF MELTING KINETICS IN RANDOMLY PACKED STEEL SCRAP IN ELECTRIC ARC FURNACE STEEL MAKING

By

HANDE AKSEKI, B.Sc.

A Thesis

Submitted to the School of Graduate Studies

in Partial Fulfillment of the Requirements

For the Degree

Master of Applied Science

McMaster University

MASTER OF APPLIED SCIENCE (2010) McMaster University

(Materials Science and Engineering) Hamilton, Ontario

TITLE: Scaling Analysis of Melting Kinetics in Randomly Packed Steel Scrap in Electric Arc Furnace Steel Making

AUTHOR: Hande Akseki, B. Sc.

SUPERVISOR: Professor Nikolas Provatas

NUMBER OF PAGES: xiv, 86

ABSTRACT

This thesis report the results of a simulation study of the melting kinetics of multiple, randomly distributed, steel scrap pieces. The model used is that previously developed by Li [Li, 2006]. The aim of this study was to better understand the universal features governing the kinetics of multi-piece scrap melting in a liquid pool. We observed the formation of a solidified shell and interfacial gap both in a single scrap piece as well as in randomly distributed multiple scrap melting cases. It is shown that the multiple scrap pieces agglomerate throughout the sample due to solidified shell formation.

The key factors affecting melting kinetics of a heat examined were: heat transfer coefficient, initial solid fraction, initial liquid (preheating) and solid temperatures, scrap size and thermal conductivity.

A scaling analysis of simulation data of melting kinetics was conducted, identifying suitable characteristic length and time scales through which the melting kinetics across different parameters and processing conditions could be scaled and thus understood in the context of a unified mathematical description.

ACKNOWLEDGMENTS

I sincerely acknowledge my supervisor Dr. Nikolas Provatas for his genuine support, guidance and patience with friendly and encouraging attitude. Dr. Provatas, as teacher and mentor, did not only help me to improve my academic skills, but also he has always strongly encouraged and supported academic independence as researcher, which helped me to increase my creative thinking abilities and provide me with real graduate school experience.

I would like thank Computational Materials Science Group of McMaster University of which I am honored to be a part.

I am really grateful to Dr. Jianghua Li for his valuable advice and support throughout this work.

I gratefully acknowledge McMaster Steel Research Centre for the financial support.

To my mom and dad, my best encouragers, thank you for everything. I would like to dedicate this thesis to my beloved parents.

TABLE OF CONTENTS

LIST OF FIGURES

Chapter 2

Chapter 3

Chapter 4

LIST OF TABLES

Chapter 4

LIST OF SYMBOLS

A_{ini}	Initial area of an average piece
A_{max}	Maximum area of an average piece
C_0	Initial carbon content of steel sample
C_L	Initial carbon content of liquid steel bath
C_s^*	Equilibrium carbon content from solidus side of Fe-C phase diagram
C_L^*	Equilibrium carbon content from liquidus side of Fe-C phase diagram
C_P	Specific heat capacity of solid/liquid steel at constant pressure
d	Instantaneous sample diameter during melting
d_0	Initial sample diameter
D	Mass diffusion coefficient
D_{AB}	Binary mass diffusion coefficient
F	Free energy functional in phase field model
h	Heat transfer coefficient
h_{still}	Heat transfer coefficient for still interface
$\widetilde{h}$	Heat transfer coefficient in phase field model
h_m	Mass transfer coefficient
k_0	Initial value of thermal conductivity
k	Thermal conductivity of solid steel

k_L	Thermal conductivity of liquid steel
k_{eff}	Thermal conductivity of interfacial gap
L	Average initial length of a scrap piece
L_{inc}	Increase in the length of an average piece
L_s	Length of the system’s square
L^*	Effective change of the length of the solidified shell around a scrap piece
N	Number of scrap pieces
r	Radius of a scrap piece
t	time
T_0	Initial steel sample temperature
T_{int}	Interface temperature
T_L	Initial liquid steel temperature
T_M	Melting temperature of steel sample
T_S	Initial solid steel temperature
V	Interface velocity
w	Interface thickness
w	Width of scrap
Gr	Grashof Number
Nu	Nusselt Number
Pr	Prandl number

Re	Reynolds number
Sc	Schmidt number
Sh	Sherwood number
α_S	Thermal diffusivity of solid steel
α_L	Thermal diffusivity of liquid steel
β	Volumetric thermal expansion coefficient
Δ_{eff}	Effective growth rate
ΔH_f	Latent heat of fusion
ρ	Density of solid/liquid steel
δ_T	Thermal boundary layer thickness
δ_C	Concentration boundary layer thickness
Φ	Phase field order parameter
μ	Viscosity
ν	Kinematic viscosity
τ	Characteristic time of phase field simulation
λ	Dimensionless parameter in phase field model

Chapter 1
Introduction

1.1 Motivation for the Thesis

Scrap heating and melting can take up to 60% of the total energy requirement in Electric Arc Furnace (EAF) steel making; as a result, it is a crucial step in the overall steel production process. Since 1965, many researchers have conducted experiments and developed mathematical models to understand and describe this process. Pehlke *et al.* [Pehlke *et al.*, 1965], Olsson [Olsson, 1965], Kosaka *et al.* [Kosaka *et al.*, 1967], Kim *et al.* [Kim *et al.*, 1974] and Wright [Wright, 1989] focused on how mass transfer controlled scrap melting. They solved simple mass transfer problem in 1D using the Lommel and Chalmers Equation [Lommel *et al.,* 1959] and empirical correlations between dimensionless groups to obtain the mass transfer coefficient. They focused on single scrap melting and on pieces with simple geometry for making calculations effectively one dimensional.

Guthrie *et al.* [Guthrie *et al.*, 1971] developed a melting model controlled by heat transfer. They conducted experiments with single hemispherical bars, which they connected to their experiments using empirical correlation groups. Since their experimental conditions differed from their theoretical assumptions, they were not able to validate their model.

Szekely *et al.* [Szekely *et al.*, 1972] conducted experiments with single bars and developed a mathematical model to solve the heat and mass equations simultaneously. They used a Green's function to solve sharp interface equations. They have used an empirical correlation to obtain a mass transfer coefficient, but did not report enough experimental results to validate their model.

Gaye *et al.* [Gaye *et al.*, 1985] conducted multi-piece melting experiments and developed a mathematical model solving the heat and mass equations simultaneously for multi-piece melting. They mentioned the importance of the solidification stage and interface emerging, but because of the nature of the sharp interface model, they were not able to develop a successful model to capture the solidification stage of scrap melting.

Li [Li, 2006] conducted experiments with one and two bars, and he developed a new type continuum model which couples the heat transfer equation and so-called phase field approach. He used a semi empirical correlation between dimensionless groups to obtain the heat transfer coefficient. His model is able to account for solidification, remelting of the solidified shell, and interface merging. Although he assumed that the heat transfer coefficient and the liquid temperature are constant, he was able to validate his model to a reasonable accuracy. He used his model to study melting in randomly packed multi-piece scrap distributions. Owing to the complexity of setting up appropriate experiments the random scrap melting has yet to be validated. The above quick summary of some of the more successful models of scrap melting indicate that our understanding of the kinetics of scrap melting in EAF steel making is far from complete, particularly in regard to randomly packed multi-piece scrap melting.

1.2 Objectives of the Study

This work will use the model of Li [Li, 2006] to investigate and characterize the melting kinetics of scrap melting in a liquid pool. The model is chosen due to its unique ability to self-consistently simulate free boundary motion and interface agglomeration alongside the heat transfer kinetics of melting. This model is also chosen as it is presently the only type that has been validated for single and double bar experiments. Key effects addressed in this thesis include:

- Effect of packing density of scrap on melting
- Effect of stirring (heat transfer coefficient) on melting
- Effect of liquid steel bath temperature on melting
- Effect of scrap preheating on melting
- Effect of thermal conductivity on melting
- Effect of scrap size on melting

After characterizing the above effects on multiple scrap piece melting in the liquid pool a scaling analysis of the data is constructed, which will allow the generic features of the scrap melting process to be characterized via dimensionless groupings of variables, constructed to elucidate characteristic times and length scales inherent to the scrap melting phenomenon.

1.3 Organization of the Thesis

The content of this thesis is organized as five chapters. Chapter 1 outlines the motivation and objectives of the research. In Chapter 2, the basic theory of the scrap melting and previous research done in this area is presented. Chapter 3 outlines the model and the simulation methodology used in this work. In Chapter 4, the results of the simulations are shown and the new scaling approach to the problem is presented. Chapter 5 summarizes the current research and highlights the main conclusions.

Chapter 2
Literature Review

2.1 Steel and the Steel Manufacture

Steel is one of the most important materials in the world and one of the most widely produced with over trillion tons of annual production [Thecanadianencyclopedia.com, 2010]. Steel has been produced in Canada since the 1880's and 14.9 million tons of steel were produced in Canada in 2008 which brought 14 billion dollars of income to the country and provided 30,000 people with jobs [Canadiansteel.ca, 2010].

Steel is an iron alloy consisting of 0.2-2% carbon by weight. Manganese, silicon, chrome and nickel are the common alloy additions to improve the quality of steel with respect to corrosion resistance, hardness and other properties.

The amount of carbon in the alloy has a tremendous impact on steel's properties. Generally, more carbon means better strength but poor welding characteristics and toughness.

There are two methods for steel production. The first one is the integrated steelmaking approach. The raw material, iron ore, is crushed, sintered and bonded. The solid pieces of iron ore are fed to the Blast Furnace with coke. Very hot air (~1200° C) streaming from the bottom of the furnace causes the combustion of coke to carbon oxides which reduces the iron oxide to iron. The iron melts with the heat created by combustion. This molten iron is called pig iron. At the last step of integrated steelmaking, the unwanted substances (carbon, residues) are burned off with the help of pure oxygen in a Basic Oxygen Furnace (BOF).

Alternatively, steel can be produced through Electric Arc Furnace (EAF) steelmaking without using hot metal. The raw material in EAF steelmaking is recycled steel scrap. Scrap first melts with the heat obtained from electrical and chemical energy, and is then refined to produce steel.

Given the competitive nature of today's industry, Electric Arc Furnace steelmaking has significant importance because of its high production speed, consistent quality, and low production costs. The lower energy consumption and equipment investment as compared to integrated steel making favors the EAF process in areas where scrap steel and electric power supply are available. Additionally EAF steel making plays an important role in driving the recovery and recycling of waste iron, while integrated steel making facilities have more serious negative environmental impacts.

There are two major types of EAF: an Alternating Current (AC) Arc Furnace (Figure 2-1) uses three graphite electrodes to create an arc and heat the scrap by alternating current: a Direct Current (DC) Arc Furnace has only one graphite electrode in the centre which acts like a cathode and while the furnace bottom acts like an anode.

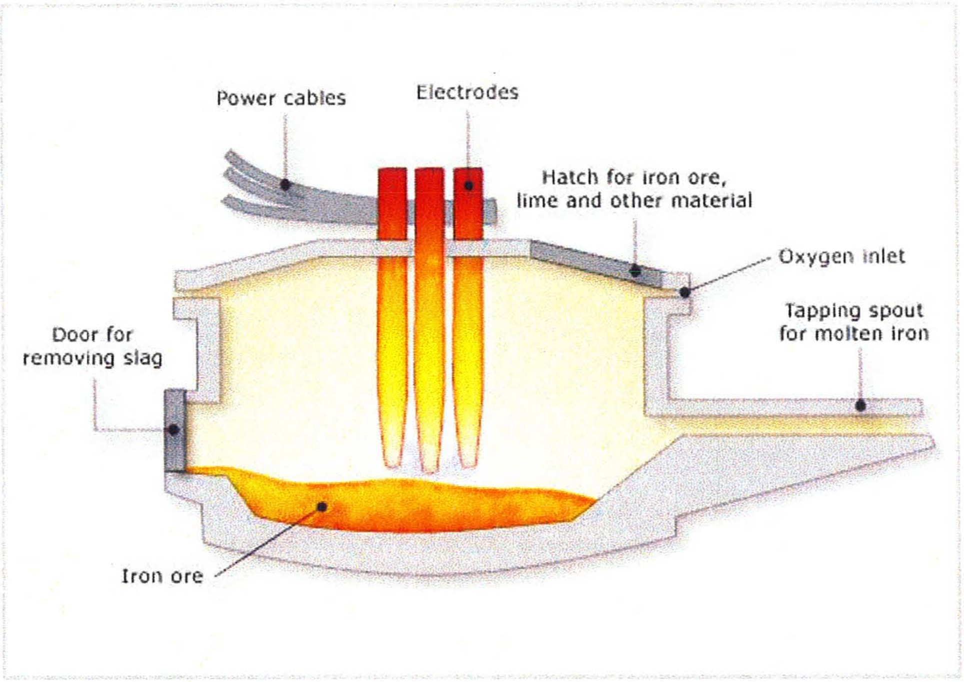

Figure 2-1: Schematic diagram of an AC Electric Arc Furnace

(http://www.teara.govt.nz/en/iron-and-steel/2/4)

(1) Scrap

Steel scrap is the main raw material of EAF operation. There are two types of scrap steel [Steeluniversity.org, 2010]:

1. Internal scrap, produced by different processes inside the steel mill and not used as a part of final product.
2. Merchant scrap, commercially available in the scrap market.

Scrap is classified according to chemical composition, level of impurity, size, shape and homogeneity (variation within given specifications).

Figure 2-2: Steel scrap pieces of different sizes and geometries

(http://www.caltechcorp.com/8.html)

(2) Operation

During the EAF operations, the steel scrap pieces are melted in batches which are known as "heats" [Steel.org, 2010]. The EAF operation cycle is called the tap to tap cycle and consists of charging, melting, refining, deslagging and tapping steps. The first step is charging. Scrap is layered according to size and density before charging to obtain proper melting conditions. In most operations, two or three buckets of scrap are charged per heat. Lighter scrap pieces are placed on the bottom part of the EAF since they act like a cushion and protect the furnace from damage caused by heavy lumps of scrap. It is also important to charge lighter scrap pieces to the top of the EAF, since they favor the boring of electrodes. Heavy and medium pieces are placed under a layer of light scrap since they can cause electrode breakage by physical contact and leveling delays if they are placed on the top.

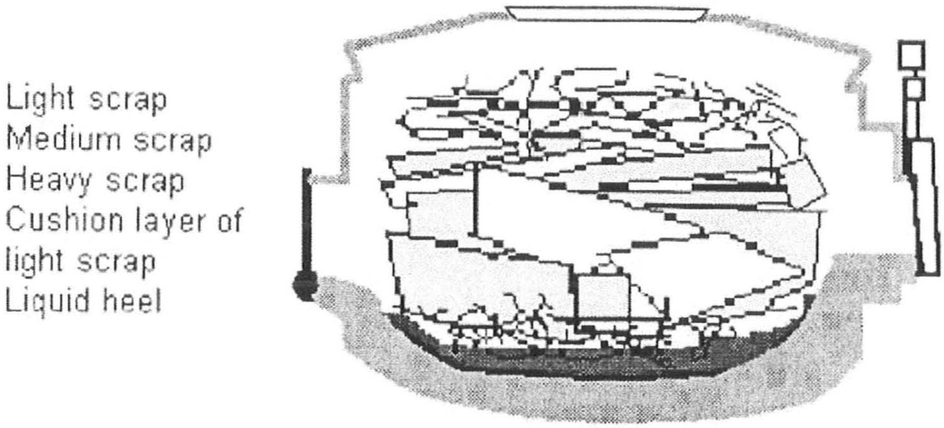

Figure 2-3: Correctly charged furnace [Ostman, 2006]

Melting is the second step, which usually takes more than the half of tap to tap time in an operation cycle.

The main heat source for melting is electric energy supplied by the graphite electrodes. Although traditionally the power usage of the EAF was above 600 kWh/mt [Fruehan, 1985], development in technology allows steelmakers to reduce the consumption to the range of 380-400 kWh/mt [Gripenberg *et al.*, 1990]. After combustion in the EAF, EAF bath stirring [Baukal *et al.*, 1990], scrap preheating [Rudzki *et al.*, 1972; Rudzki *et al.*, 1973; Franklin, 1991], the use of burners inside the EAF [Baukal *et al.*, 1990; Shifrin *et al.*, 2001; Thomson *et al.*, 2001; Teoh, 1989; Adolph *et al.*, 1989; Wells *et al.*, 1986] and post combustion [Li, 2003; Tang *et al.*, 2003] also contribute in order to reduce energy consumption.

Chemical energy also contributes to melting, supplied via fuel-air burners (burning natural gas and air) or oxy fuel burners (burning natural gas and oxygen). After melting is completed, the refining stage starts. During the refining stage unwanted substances like carbon, phosphorus, aluminum, and silicon are removed with the injection of the oxygen. After completing the refining stage, the molten steel is tapped into the ladle and the next batch operation starts.

Scrap melting in EAF can be divided into three stages [Ostman, 2006]:

1. The heating starts just after the scrap pieces fall into the furnace. Scrap pieces are heated by hot gases inside the furnace and electric arcs striking between electrodes and metal. During the heating stage, heat is transferred from gas to solid-state material.
2. When the scrap pieces on the top reach their melting points, the melting stage starts. The liquid metal droplets pool on the bottom of the furnace. During the melting stage, the liquid-solid, solid-gas, and gas liquid interfaces exist simultaneously. Solid scrap pieces are heated by hot gases and the electric arcs, as well as the hot liquid metal.
3. The finishing stage starts when all the scrap pieces are immersed in the liquid metal pool. During the finishing stage there is no further solid-gas interaction and all remaining scrap pieces are heated by surrounding liquid metal.

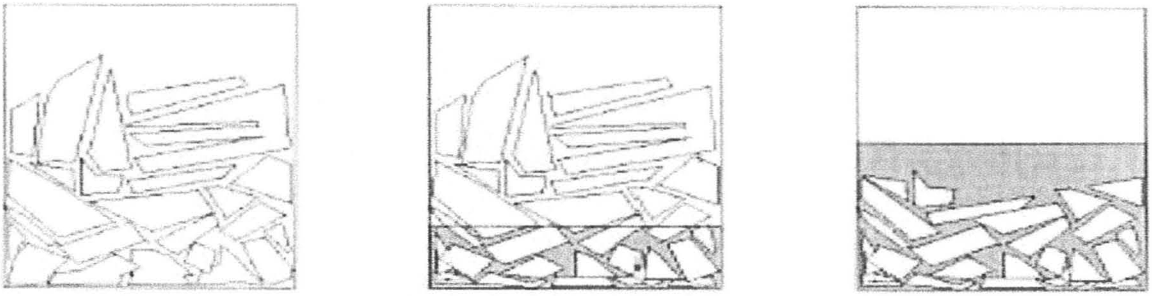

1. Heating 2. Melting 3. Finishing

Figure 2-4: Stages of melting in an EAF [Ostman, 2006]

This thesis focuses on mathematical modeling of the melting of scrap pieces inside of the liquid pool, during the stage where only a solid-liquid interface exists.

2.2 Sharp Interface Model

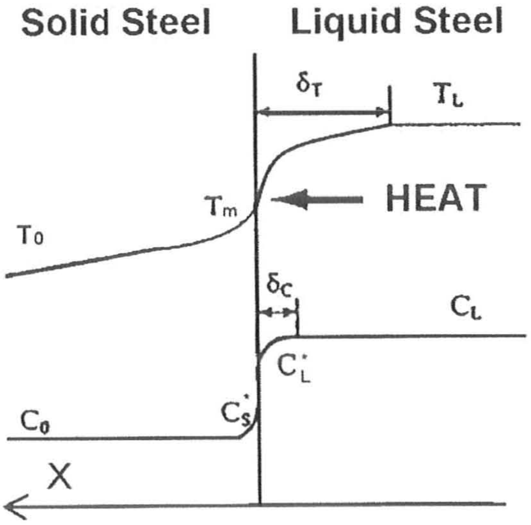

Figure 2-5: The temperature and concentration profile of liquid-solid interface [Li, 2006]

If a solid scrap piece having carbon concentration of C_0 and temperature of T_0 is immersed in a hot liquid bath having carbon concentration of C_L and temperature of T_L, the temperature on the interface (T_m) will differ from T_0 and T_L. Also, the carbon concentrations on the interface C_s^* and C_L^* will differ according to the iron carbon phase diagram. 99% of the heat and mass transfer occurs inside of the boundary layers δ_T and δ_C [Incorpera *et al.*, 2002]. The heat flow in the liquid phase is determined according to the thickness and the characteristics of the given boundary layers. Heat transfer inside the solid can be described by the conduction equation:

$$\frac{\partial T}{\partial t} = \frac{k}{C_p \rho} \frac{\partial^2 T}{\partial x^2} \qquad (2.1\text{ a})$$

This equation can be expressed in cylindrical and spherical coordinates as:

$$\frac{\partial T}{\partial t} = \alpha_s \left(\frac{\partial^2 T}{\partial r^2} + \frac{n}{r}\frac{\partial T}{\partial r}\right), 0 < r \le R(t) \qquad (2.1\text{ b})$$

where n=1 for cylinders and n=2 for spheres, r is the radius of the scrap piece, α_s is the thermal diffusivity and $R(t)$ is the position of the liquid solid interface.

The heat balance at the interface can be expressed as:

$$h(T_L - T_S) = \rho \Delta H_f V - k \left.\frac{\partial T_S}{\partial x}\right|_{\text{int}} \qquad (2.2)$$

where h represents the heat transfer coefficient between the solid and the liquid, V represents the interface velocity, and ΔH_f is the latent of fusion.

In equation 2.2, the first term represents the heat flux supplied by the liquid, the second term represents the heat flux used for melting and the third term represents the heat flux dissipated in the solid. If equation 2.2 examined carefully, it can be seen that just after the cold piece is immersed in to the hot liquid bath the heat flux dissipated in the solid term would be larger than the heat flux supplied by the liquid term. This suggests that a solidification stage should occur before the melting stage starts. This phenomenon is also observed experimentally [Li, 2006; Gaye *et al.*, 1985].

The mass balance on the interface can be presented as:

$$h_m(C_L - C_L^*) = (C_L^* - C_s^*)V - D\left.\frac{\partial C}{\partial x}\right|_{\text{int}} \tag{2.3}$$

where D expresses the mass diffusion coefficient between carbon and the scrap and h_m represents the mass transfer coefficient between liquid and solid.

Sharp interface models involving one or more sharp interface equations such as those in Equations (2.2) and (2.3) are notoriously difficult to simulate numerically in two and three spatial dimensions due to the complex topology of interfaces and interface merging or pinch-off.

To our knowledge, previous researchers modeling the melting of scrap in the liquid pool used the traditional sharp interface model except Li [Li, 2006]. Li coupled the heat transfer equation of sharp interface model with a new front-evolving equation that originates -at least in spirit- in the so-called phase field method. The phase field equation is constructed to track phase changes from liquid to solid and the accompanying change of interfaces. This methodology and model will be the method of choice for the study in this work and will be reviewed in later sections.

2.3 Mechanisms of Scrap Melting in a Liquid Pool

As stated by Gaye *et al.* [Gaye *et al.*, 1985] the process of melting of the scrap in the liquid bath can occur in three different ways:

a. The process can be governed by the mass transfer. To achieve this mechanism:
    i. The carbon concentration of the liquid bath should be different than the carbon concentration of the solid scrap.
    ii. The heat transfer should be faster than mass transfer.
b. The melting process can be governed by heat transfer. In this case, the carbon concentration of the liquid and solid should be approximately equal to each other.
c. Third and most realistic mechanism governing melting process is simultaneous consideration of mass and heat transfer.

2.3.1 Mass Transfer Controlled Melting

As stated above, the melting process is dominated by mass transfer if carbon concentration of the solid and liquid are not equal to each other and the heat transfer occurs much faster than the mass transfer. To be able to model mass transfer controlled melting, mass transfer equation and Equation 2.3 need to be solved. In almost all papers the last term ($D\left.\frac{\partial C}{\partial x}\right|_{\text{int}}$) in equation 2.3 has been neglected by assuming the carbon diffusion inside the solid is smaller than the thermal diffusion.

Many researchers including Pehlke et al. [Pehlke *et al.*, 1965], Olsson [Olsson, 1965], Kosaka *et al* [Kosaka *et al.,* 1967], Kim *et al.* [Kim *et al.,* 1974], and Wright [Wright, 1989] investigated mass transfer dominated scrap melting. Understanding mass transfer controlled melting processes are important to understand especially BOF (Basic Oxygen Furnace), since in BOF process the liquid carbon concentration (4-5%) is dramatically higher than the solid scrap pieces' carbon concentration (0.1-0.4%). Another phenomenon to be understood is the melting temperature decrease caused by the carbon diffusion. As Szekely *et al.* [Szekely *et al.*, 1972] showed that the diffusion of carbon atoms from the liquid to solid lowers the melting point of the scrap pieces.

In the next part of the work, the effect of different convection mechanisms to melting will be discussed.

i. Natural Convection

Kim *et al.* [Kim *et al.,* 1974] conducted melting experiments with vertical cylinders (R=1.27 cm) of 1045 steel in an iron bath (isothermal conditions). The results suggested that melting rates are increasing with increasing liquid temperature (see Figure 2-6).

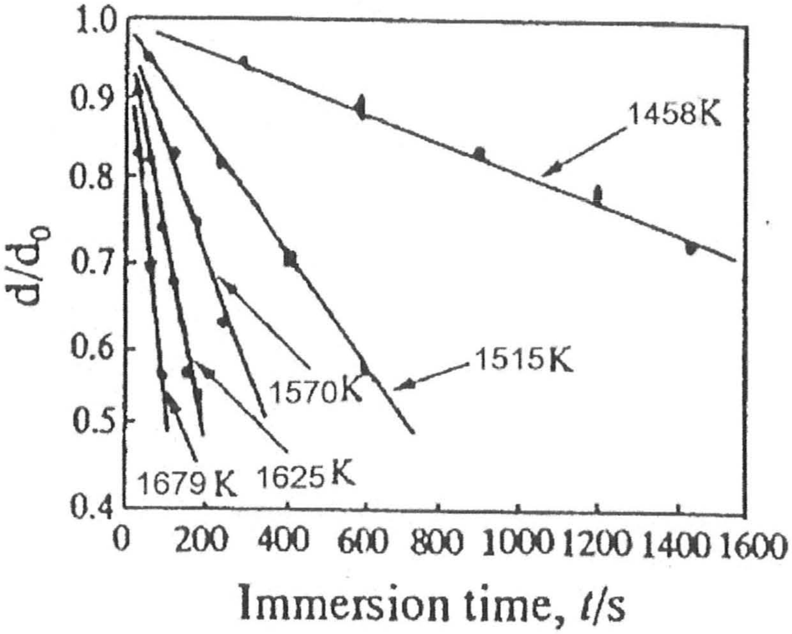

Figure 2-6: Dissolution of 1045 steel rods in molten iron bath [Kim *et al.*, 1974]

Wright [Wright, 1989] conducted melting experiment with steel cylinders having carbon concentration of 0.27-0.6% to stagnant bath having carbon concentration of 2-4.5wt% (isothermal conditions). According to his results, the melting rate increases with increasing carbon concentration of the liquid bath (see Figure 2-7). These results provide evidence for the theory that carbon diffusion causes a decrease in melting temperature.

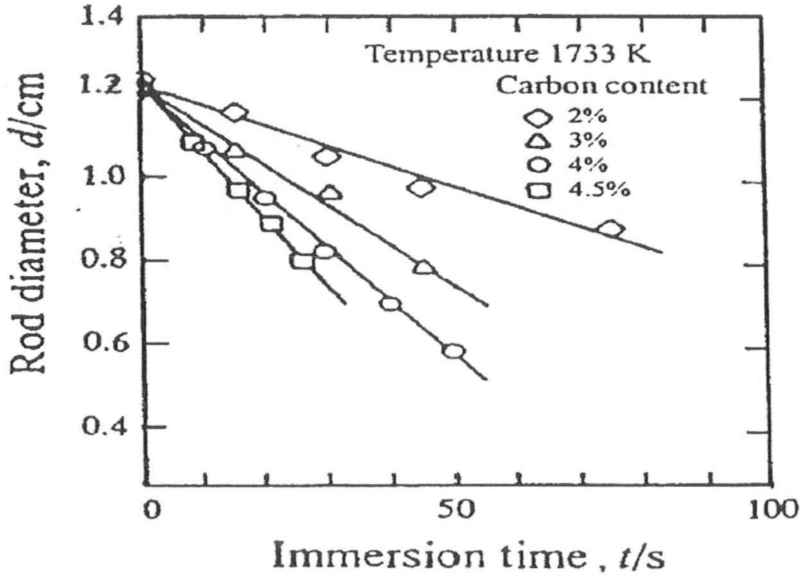

Figure 2-7: Effect of carbon content on dissolution rate [Wright, 1989]

Both researchers have used the Lommel and Chalmers Equation to obtain the mass transfer coefficient (h_m) from the slope of the melting rate curve.

$$\frac{dr}{dt} = h_m \ln[1 + \frac{C_L - C_L^*}{C_L^* - C_s}] \qquad (2.4)$$

To obtain h_m in natural convection, several dimensionless groups can be used:

Sherwood Number: $Sh = \frac{h_m L}{D_{AB}}$

Reynolds Number: $\mathrm{Re} = \frac{VL}{\nu}$

Schmidt Number: $Sc = \frac{\nu}{D_{AB}}$

Grashof Number: $Gr_m = \frac{\beta(T_m - T_L) g L^3}{\nu^2}$

Raleigh Number: $Ra = \mathrm{Re}\, Gr$

where L is the characteristic length, D_{AB} is the binary mass diffusion coefficient, β is the thermal expansion coefficient, V is the velocity v is the kinematic viscosity and g is the gravity of Earth.

In order to incorporate the effect of mass transfer, generally the following correlation is used where a and m are constants:

$$Sh = a(Gr_m Sc)^m \tag{2.5}$$

Different researchers obtained different empirical correlations by using different experimental conditions.

Kim *et al.* [Kim *et al,* 1974] obtained ($60<Sh<120$ and $6.9*10^8<Gr_mSc<7.7*10^9$):

$$Sh = 0.149(Gr_m Sc)^{0.294} \tag{2.6}$$

Wright [Wright, 1989] obtained ($142<Sh<195$ and $Gr_mSc>10^9$):

$$Sh = 0.13(Gr_m Sc)^{0.34} \tag{2.7}$$

And Kosaka et al. [Kosaka *et al.,* 1967] obtained ($10^9<Gr_mSc<10^{11}$)

$$Sh = 0.11(Gr_m Sc)^{0.33} \tag{2.8}$$

The above empirical correlations have been summarized by Brabie *et al.* [Brabie *et al.*, 2000] as seen in Figure 2-8.

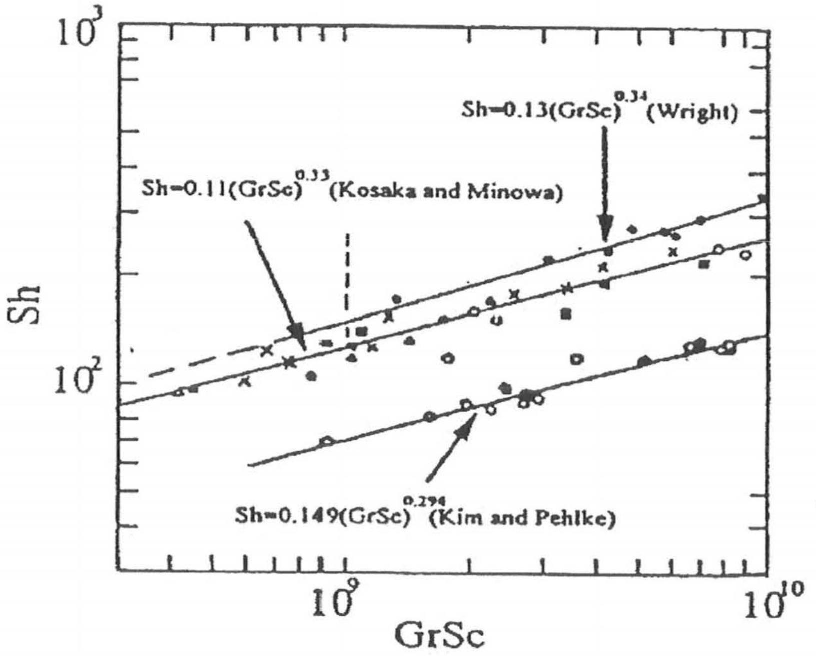

Figure 2-8: Correlations between Sh and GrSc according different researchers [Brabie *et al.*, 2000]

ii. Forced Convection

Olsson [Olsson, 1965] conducted melting experiments under forced convection condition. He used cylindrical scrap pieces with 0.0081 and 1 wt% C under isothermal conditions. In his experiments the scrap pieces was rotating to create a forced convection environment. To calculate the mass transfer coefficient, the Lommel and Chalmers Equation (2.4) was used. To following correlation is obtained to describe the mass transfer coefficient and peripheral velocity (V):

$$h_m = const(V)^{0.7} \qquad (2.9)$$

Kim *et al.* [Kim *et al,* 1974] obtained a similar relationship between mass transfer coefficient and the fluid velocity (V):

$$h_m = const(V)^{0.67} \tag{2.10}$$

Wright [Wright, 1989] researched the correlation between the mass transfer coefficient and gas injection flow rate, obtaining (see Figure 2-9):

$$h_m = const(V)^{0.21} \tag{2.11}$$

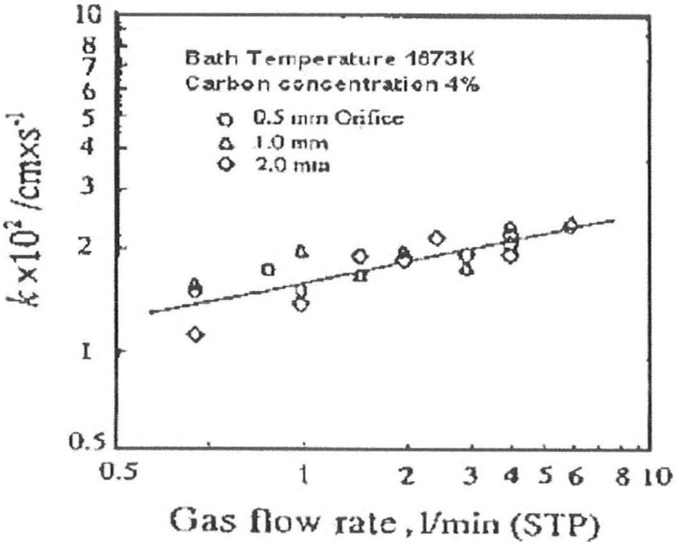

Figure 2-9: Relationship between mass transfer coefficient and gas flow rate [Wright, 1989]

2.3.2 Heat Transfer Controlled Melting

As stated above, scrap melting in the liquid bath is controlled predominately by heat transfer when the carbon concentration of the solid and liquid are equal.

One of the first investigations focusing on heat transfer controlled melting is Guthrie et al. [Guthrie *et al.,* 1971]. They have investigated the effect of superheat, preheat, thermal properties and the bath temperature to the melting kinetics of iron spheres. They solved equations 2.1 b (since they assumed their scrap pieces are radial) and 2.2 to obtain their mathematical model. They also assumed that there are no chemical interactions between impurities and bath, the material properties of the liquid bath and the solid pieces were equal , the heats of solution is zero and heat transfer is controlled by natural convection. They have used the following dimensionless groups:

Nusselt Number: $$Nu = \frac{hL_C}{k_L} \qquad (2.12)$$

Prandtl Number: $$\Pr = \frac{\nu}{\alpha_L} \qquad (2.13)$$

They devised the following empirical equation to obtain the heat transfer coefficient:

$$Nu = 0.539[\frac{\Pr}{0.952+\Pr} x(Gr\Pr)]^{0.25} \qquad (2.14)$$

The comparison between their experimental and theoretic results can be found in Figure 2-10. As seen from the figure there is qualitative agreement, but the experimental and theoretical results differ from each other quantitatively.

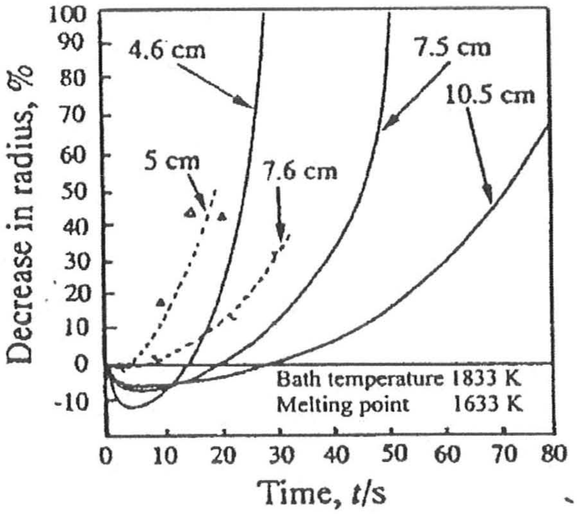

Figure 2-10: Theoretical (solid lines) and experimental (dotted lines) results [Guthrie *et al.,* 1971]

Possible causes of error include:

1. Although hemispheres were used in the experiments, their model assumes spherical pieces.
2. The carbon concentration of liquid and solid were different in their experiments.

Li [Li, 2006] has conducted experiments with cylindrical bars having diameters of 25.4mm, 31.8mm and 38.1mm, and he investigated the effect of superheat, preheat, size and shape of the bars. Also, he conducted experiments with two bars having a diameter of 25.4mm. To investigate the effect of spacing in scrap melting, he has used bars having different spacing from 1.27mm to 6.35mm. To model the melting kinetics of his experiments, Li used a very different approach, based on an adaptation of the phase field method. The strength of his model allowed him to simulate the melting of multiple scrap pieces and scrap pieces having complex topologies. Also, his model was able to capture the solidification stage that occurs before melting and the agglomeration of the pieces caused by primary solidification. This model will be explained in detail in Chapter 3. Only selected results of his work are shown here.

Figures 2-11, 2-12 and 2-13 show a comparison of Li's modeling work and experiments he conducted to validate their model for single piece scrap melting. Figure-11 shows a comparison of Li's experimental and modeling results for single scrap pieces having different preheating temperatures, Figure 2-12 shows the same comparison for scrap pieces having different diameters. In Figure 2-13, the experimental-theoretical comparison is presented for two bars having different spacings.

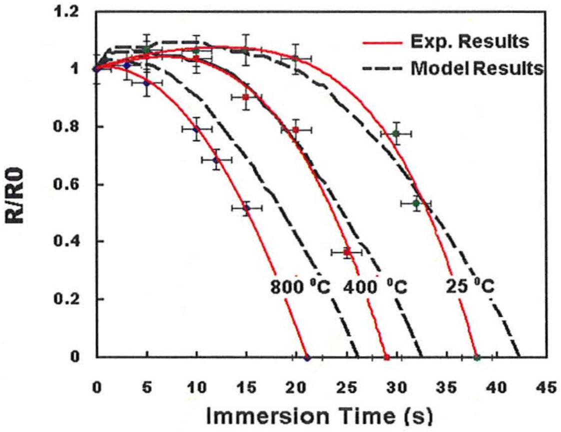

Figure 2-11: Comparison between experimental and theoretical results for pieces having different preheating T [Li, 2006]

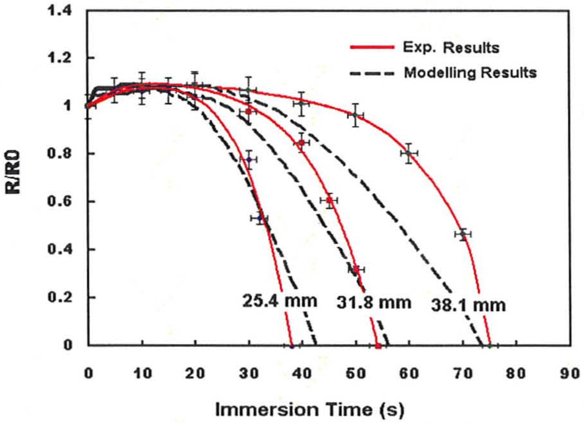

Figure 2-12: Comparison between experimental and theoretical results for pieces having different diameters [Li, 2006]

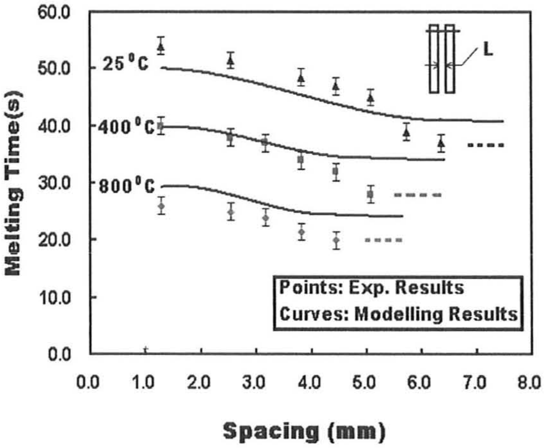

Figure 2-13: Comparison between experimental and theoretical results for two pieces having different preheating T and different spacings [Li, 2006]

The phase field method for modeling of scrap melting has enjoyed a significant success, as the method is capable of handling free boundary motion and merging (see Figure 2-14), and it is validated experimentally for single and double bar configurations. In this work, the model of Li is used to model the multiple scrap melting and to study the universal behavior of scrap melting in liquid pools. At present, there is no experimental data available to validate multiple melting results.

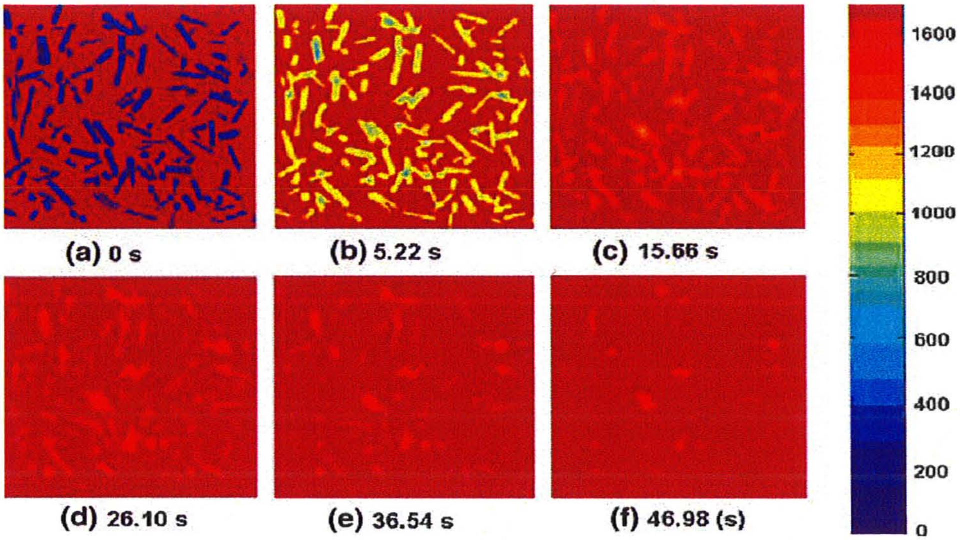
(a) 0 s (b) 5.22 s (c) 15.66 s

(d) 26.10 s (e) 36.54 s (f) 46.98 (s)

Figure 2-14: Phase field model results for multiple melting simulations [Li, 2006]

The model of Li has the following weaknesses:

1. Although the temperature of the liquid changed with time, the model assumed a constant temperature.
2. The heat transfer coefficient should reflect changes in temperature and solid fraction. However, this was also assumed to be constant.
3. Interfacial heat resistance between the solidified shell and the original bar is determined phenomenologically.
4. After the pieces become small, the model loses its accuracy since the sizes of scraps become comparable to grid size and the model-imposed interface width.

2.3.3 Heat and Mass Transfer Controlled Melting

As indicated above, in most instances melting in a molten bath is controlled by heat and mass transfer simultaneously. Szekely et al. [Szekely *et al.*, 1972] conducted experiments with cylindrical bars having carbon concentration of 0.22wt%-0.27wt% in a molten bath having carbon concentration of 2.5wt%wt-4.4wt%. They solved Equations 2.1 and 2.2 using Green's function method. In the model, the melting point is described with the following equation:

$$T_m[°C] = 1540 - 8.3x10^3 * C_L^* \qquad 0 \leq C_L^* \leq 4\% \qquad (2.15)$$

where C_L^* is the equilibrium concentration and can be presented as:

$$C_L^* = \frac{h_m[C_L - C_L^*]}{\left|\frac{dr}{dt}\right| + h_m[C_L - C_L^*]} \qquad (2.16)$$

Equation 2.16 is simply the Lommel and Chalmers equation as modified by Szekely *et. al* [Szekely *et. al*, 1972].

Szekely *et al.* [Szekely *et al.*, 1972] assumed that $\frac{dr}{dt} >> h_m\ [C_L - C_L^*]$ and decided to use the following equation:

$$T_m[°C] = 1540 - 8.3x10^3 * \frac{h_m C_L}{\left|\frac{dr}{dt}\right| + h_m} \qquad (2.17)$$

To obtain h_m, they used the following equation:

$$\frac{h_m}{h} = Sc^{0.33}\,\mathrm{Pr}^{-0.8}\, D/_{k_L} \qquad (2.18)$$

The figure below compares the experimental and theoretical results of the study. As can be seen, there is not enough experimental data to validate the model.

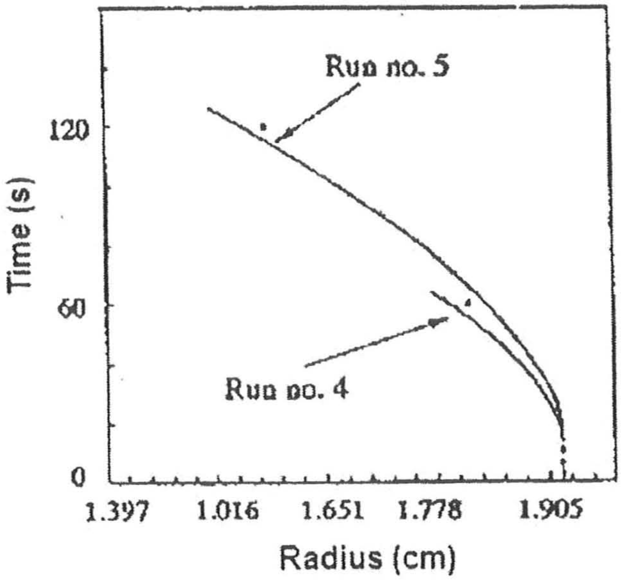

Figure 2-15: Comparison between experimental and theoretical results [Szekely *et al.,* 1972]

Gaye *et al.* [Gaye *et al,* 1985] conducted multi-piece scrap melting experiments with low C samples having diameter of 100 and 200 mm and pig iron samples having diameters of 200 mm. Gaye *et al.* mentioned that there is a solidification stage before melting, and solidification and melting the solidified shell can take up to 80% of the total melting time. They developed a model by solving equations 2.1, 2.2 and 2.3. Like researchers before him, Gaye was not able to present a multi-piece melting model capturing solidification, remelting of the solidified shell and interface merging.

Chapter 3
Modeling Methodology

3.1 Introduction

Until the study of Li [Li, 2006], researchers generally relied on the use of the 1D sharp interface model of Equations 2.1-2.3 to investigate the kinetics of melting in single pieces of steel scrap. As stated in Chapter 2, Li used the phase field method to model multi-scrap piece melting with significant success, as the method was capable of handling free boundary motion and merging (see Figures 3-1 and 3-2), and it was validated experimentally for single and double bar configurations. In this work, the model of Li is used to model multiple, randomly packed scrap melting and to study the universal behavior of scrap melting in liquid pools. This chapter reviews the basic properties of the phase field model of Li and its application to this work.

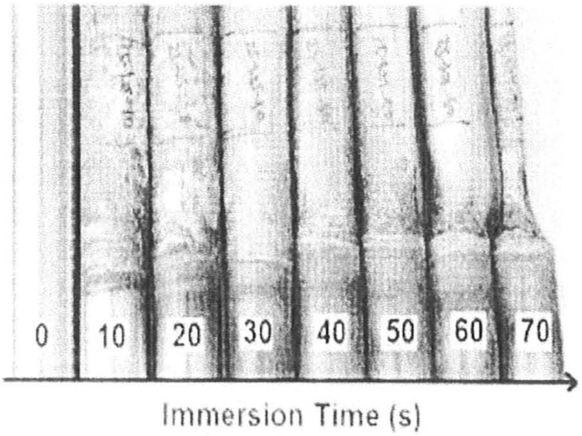

Figure 3-1: Change in the diameter of the bars with increasing time [Li, 2006]

3.2 Continuum Model of Scrap Melting

Figure 3-2: Agglomeration of two bars with increasing time [Li, 2006]

In the phase field method, an order parameter Φ is introduced. Φ can be described, loosely speaking, as the degree of crystallinity which has a constant values in the bulk phases (-1 in the liquid and 1 in the solid in our case). Within the interface, Φ varies continuously between -1 to 1. In the phase field model, the interface is not a sharp line; instead it is a region where the phase turns from solid to liquid (or from liquid to solid) smoothly.

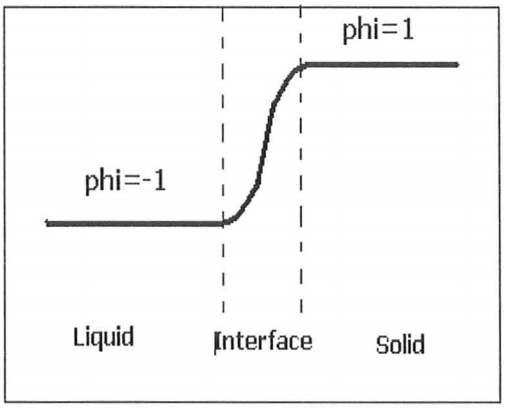

Figure 3-3: Schematic diagram of Φ field [Li, 2006]

The evolution of the phase field phi is given by the equation:

$$\tau \frac{\partial \phi}{\partial t} = w^2 \nabla^2 \phi + \phi - \phi^3 - \lambda \left(\frac{T - T_M}{\Delta H_f / C_p} \right) (1 - \phi^2)^2 \tag{3.1}$$

Where τ the characteristic time scale of the problem, w is the interface width, λ is a dimensionless parameter coupling the temperature and Φ. ΔH_f is the latent heat of fusion and C_p is the specific heat capacity. As shown in Figure 3-3, Equation 3.1 sustains moving front solutions with to stable states that are steady states of the right hand side of the equation, and the velocity of which is determined by the last term on the right hand side of Equation 3.1, which is dependent on the superheat or supercooling (T_m is the melting point). See Li [Li, 2006] for details of this equation.

A moving front generates or absorbs latent heat. This link is made in the model by associating the source of latent heat to a term proportional to $\frac{\partial \phi}{\partial t}$. The transport of heat is thus given by the equation:

$$\frac{\partial T}{\partial t} = \nabla(\alpha(\phi,T)\nabla T) + \frac{1}{2}\frac{\Delta H_f}{C_p}\frac{\partial \phi}{\partial t} + \tilde{h}(T_L - T_M)|\nabla \phi| \qquad (3.2)$$

First term on the right hand side of the phase field equation describes heat diffusion, the second term represents the latent heat, which only becomes effective on the interface; and third term represents the convection which only becomes effective on the interface as well. $\tilde{h}$ is the heat transfer coefficient in the phase field model which is proportional to the heat transfer coefficient in the sharp interface model. The proportionality can be presented as:

$$\tilde{h} = \frac{3\sqrt{2}}{4}\frac{h}{\rho C_P} \qquad (3.3)$$

The relation in Equation 3.3 comes out of a lowest order asymptotic analysis conducted by Li [Li, 2006] in which the phase field model is mapped onto the sharp interface model in the mathematical limit of W→0.

As shown in Li [Li, 2006], Li used the following two semi-empirical equations to calculate the heat transfer coefficient: (The correlations are taken from Gaye *et al.,* (Gaye *et al,* 1985))

$$Nu = \frac{h_{still}L_C}{k} = 0.686(Gr.\Pr)^{0.25} \qquad (3.4)$$

\

$$h = \frac{\delta C_P v}{\exp(\delta C_p v / h_{still}) - 1} \tag{3.5}$$

The parameters w, τ and λ are chosen according to the prescription in Li such as to emulate the appropriate sharp interface model in the limit when the interface width w becomes very small compared to any other characteristic scale in the physical problem under study.

3.3 Simulation Methodology

The model presented above has a constant heat transfer coefficient and considers a constant liquid temperature (T_L). Boundary conditions are assumed to be adiabatic, and scrap distribution is assumed to be both uniform and random. A steel scrap distribution is defined by regions of Φ=1 according to a desired scrap topography.

As stated by Fruehan [Fruehan, 1985], the liquid temperature in the electric arc furnace drops during the melting process. Also, the liquid temperature in systems having larger scrap pieces drops more quickly since larger objects consume more sensible heat. Various boundary conditions can be implemented in the model to represent these conditions. It is not clear at present which are the most realistic. In this work the bulk liquid is assumed to remain at a constant temperature. While this is an oversimplification, it can nevertheless be useful in elucidating some of the basic features of scrap melting in random scrap collections.

As stated above, in the model heat is continuously injected into the scrap with the $\tilde{h}(T_L - T_m)|\nabla\phi|$ term, which is placed in the energy transport equation, and $\tilde{h}$ is the constant heat transfer coefficient proportional to the heat transfer coefficient in the sharp interface model. The heat transfer coefficient (h) is a representation of the convective flow characteristics and the liquid temperature of the environment immediately surrounding the bar. According to this description, using a constant h is acceptable if the liquid temperature and convective flow is the same throughout the entire system. Because the model assumes the liquid temperature does not change during melting, and the convective flow can also be considered constant throughout the system in one bar and two bar melting cases, use of a constant heat transfer coefficient is acceptable in both one bar and two bar melting cases.

For a multi-piece distribution, a constant heat transfer coefficient is not in general acceptable. The one plausible exception is the case of a uniformly random scrap distribution, where it is reasonable to assume isotropic properties. Therefore, a constant heat transfer coefficient is applicable in the modeling of multiple scrap melting only if the scrap pieces are distributed randomly and there is no statistical difference between each location. Otherwise, a detailed (and quite complex) fluid flow formulation should be included in the model. In this work, a random distribution is obtained by using a Monte Carlo algorithm developed by Li [Li, 2006] to simulate an experimental scrap distribution measured and characterized by Mandal *et al.* [Mandal *et al.,* 2005]. In the scrap algorithm, the following assumptions have been made:

1. The scrap pieces are rectangular
2. Length and thickness of scrap pieces fall within a given range
3. Distribution of scrap piecess are uniform and random both in position and orientation
4. Pieces do not cross each other
5. Pieces do not cross boundaries

Figure 3-4 shows the experimental porosity distribution along a given direction (x) of a scrap packing in a closed box. Li [Li, 2006] constructed the Monte Carlo algorithm to model this distribution along the x or y directions of our simulation domain.

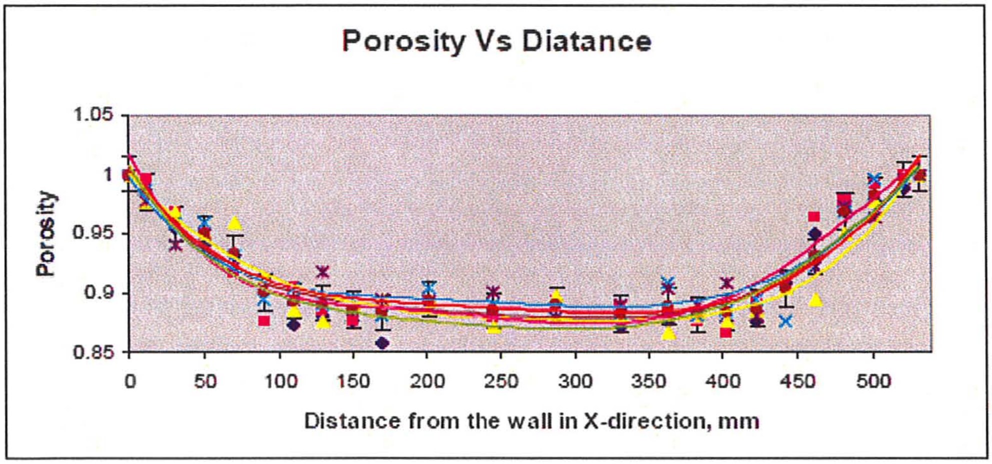

Figure 3-4: Porosity vs. Distance from Mandal *et al.*'s work [Mandal *et al.,* 2005]

3.4 Interfacial Gap and its Modeling

As stated above when a cold scrap piece is immersed into hot liquid steel, the heat flux dissipated in the solid becomes larger than the heat flux obtained from the hot liquid. This causes solidification before melting. As shown in Figure 3-5, there is a gap between the original bar and the solidified shell. This gap is believed to be caused by the imperfect contact between the solid and the liquid and also the wetting characteristics of the material. This interfacial gap has a higher heat resistance, and as shown by Li [Li, 2006], must be modeled by making the thermal conductivity spatially dependent, with an effective, time-dependent conductivity at the interface between the original bar and the solidified shell.

.

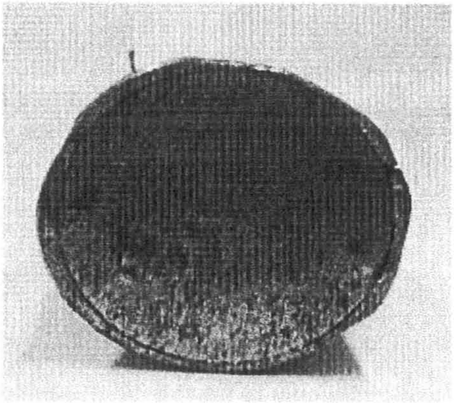

Figure 3-5: Interfacial gap between the original bar and the solidified shell [Li, 2006]

Experiments reveal that a given scrap piece reaches a maximum solid fraction and then there is period when the solid fraction does not change. This period is called the “plateau period” and is caused by the interfacial gap. The gap acts like a heat reservoir, buffering heat from the solidifying shell, thus delaying further melting of the solidified shell temporarily. The gap can therefore be seen act as a thermal resistance. Eventually, heat will get into the original bar and the bar will proceed to melt completely. To represent the heat resistance during the plateau period, a strip casting model developed by Li *et al.* [Li *et al.,* 1996] has been used. According to this model the heat conduction coefficient (k_{eff}) is constant during the plateau period. While it increases with time in order to emulate the increasing contact between the solidified shell and the original bar. Its explicit form is given by,

$$k_{eff} = k_0(1+t)^m \qquad (3.7)$$

where k_{eff} is the effective thermal conductivity

k_0 is the initial value of thermal conductivity

t is the time and,

m is a constant

It should be considered that k_{eff} is a phenomenogical thermal conductivity the precise form of which is not known. A typical form described by Equation 3.7 is shown in Figure 3-6.

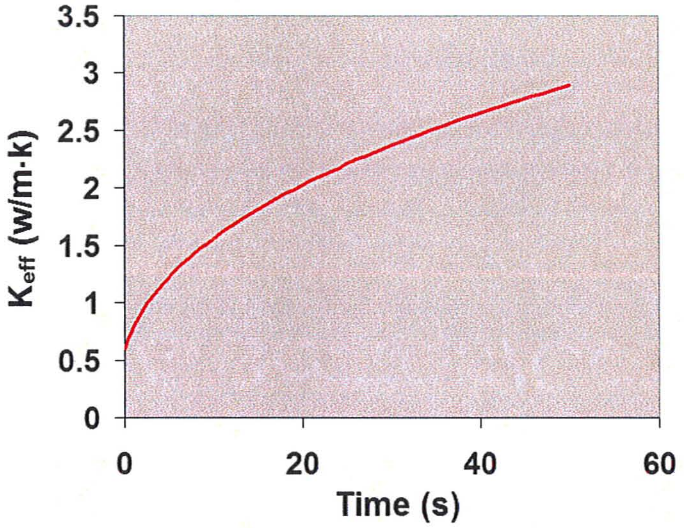

Figure 3-6: K_{eff} as a function of time

Chapter 4
Results and Discussions

4.1 Introduction

This chapter will use the scrap melting model outlined in Chapter 3 (Equations 3.1 and 3.2) to simulate the kinetics of melting in random distributions of scrap. Equations 3.1 and 3.2 were numerically solved with the simple 2D finite difference method [Landau *et al.,* 1997] used by the previous researcher [Li, 2006]. Two dimensional simulations were performed on a system, sized 0.4x0.4 m and on uniform mesh sized $\Delta x=\Delta y=0.195$ mm, model time units are set to $\tau=0.05$s, $\lambda=2$ and interface thickness parameter is chosen as $w=0.195$ mm. The materials properties given in the tables 4-1 and 4-2 are used and density and latent heat are assumed to be constant in both liquid and solid phases. Simulations were performed for different heat transfer coefficients (h), thermal conductivities (k), preheating Temperatures (T_s), liquid Temperatures (T_L), scrap sizes and initial solid fractions (ISF). A summary of parameters for which simulations were conducted is found in the Table 4-3.

Physical Properties of solid steel	
Tm(K)	1793
Cp(J/kg.K)	400 at 298 K
ρ(kg/m^3)	7750
ΔHf(J/kg)	272000

Table 4-1: Material Properties of solid 1018 steel [Lampman, 1990]

Physical Properties of the	**liquid steel**
Viscosity(N.s/m^2)	4.5 x10^{-3}
Kinematic Viscosity(m^2/s)	400 at 298 K
ρ(kg/m^3)	6900
ΔHf(J/kg)	272000
Volumetric thermal expension coefficient (K^{-1})	6.2x10^{-5}

Table 4-2: Material Properties of liquid steel at 1585°C [Kawai *et al.*, 1998]

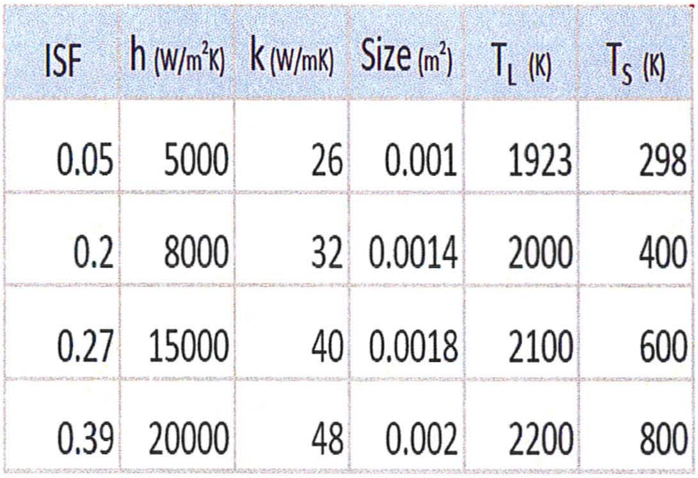

ISF	h (W/m^{2}K)	k (W/mK)	Size (m^2)	T_L (K)	T_S (K)
0.05	5000	26	0.001	1923	298
0.2	8000	32	0.0014	2000	400
0.27	15000	40	0.0018	2100	600
0.39	20000	48	0.002	2200	800

Table 4-3: Summary of the performed simulations

An example for a typical melting process simulated by the model of Chapter 3 can be seen in the figure 4-1. The figures on the left represent the phases where blue represents the liquid and red represents the solid. The figures on the right hand side represent the temperature distributions, with blue representing cold and red representing hot. Temperature scales can be found to the right of the figures. The change in the phases from solid to liquid and the temperature distribution from cold to hot are given from top to bottom as time increases. As seen from the figures, the continuum model is able to capture the solidification stage that occurs before melting and the agglomeration of pieces ("steel iceberg" formation) caused by the solidification. As seen from the figures, the scrap pieces located in denser solid piece areas create larger steel icebergs and, these take longer to melt than scrap pieces melting individually. Additionally, scrap pieces in less dense areas melt as quickly as individual pieces. The steel icebergs are the predominant factor affecting total system melting, since larger and numerous icebergs lead to longer melting time.

4.2 Effect of Input Variables on Melting

4.2.1 Effect of Initial Solid Fraction (ISF)

The first part of the study focuses on investigating the effect of Initial Sold Fraction (ISF) on melting. In this work, the ISF is calculated with the following formula:

$$ISF = N(\frac{Lw}{L_s^2}) \qquad (4.1)$$

where N is the number of scrap pieces put in the system, L is the average initial length of a scrap piece, w average initial width of a scrap piece L_s is the length of the system, where a square geometry is used in all simulations. The notation "w" refers to the width of scrap and not the characteristic boundary layer interface of the phase field equation, which will not be discussed any further.

To investigate the effect of ISF on the system, simulations were performed with four different ISF values (0.05, 0.2, 0.27, 0.39), in four different systems having four different heat transfer coefficients (5000 W/m^2K, 8000 W/m^2K, 15000 W/m^2K, 20000 W/m^2K). Thermal conductivities (k), Preheating Temperatures (T_s), Liquid Temperatures (T_L), and scrap sizes were kept the same for these runs (k=32 W/mK, T_s= 298 K, T_L=1923 K scrap size=0.001 m^2). It should be noted that, in this section, the larger ISFs are obtained by increasing the number of scrap pieces. The effect of scrap sizes on melting will be investigated below.

Figures 4-2 and 4-3 show two of the results from the first part of the investigation. The maximum solid fraction, which is represented by the peak of the curve, becomes larger with the increasing ISF. It should also be mentioned that the curves lose their linearity after decreasing to a small solid fraction. As mentioned in Chapter 3, heat is injected to the system via the term $(h \cdot A\ (T_L - T_m)$ where h, T_L and T_m are constant. The only variable changing is the interfacial area A. Therefore, during melting, when the interfacial area A becomes very small, the heat that goes in to the scrap piece decrease dramatically. This causes the breakdown of linearity at the end of the melting stage. The model is assumed to be least accurate in this stage.

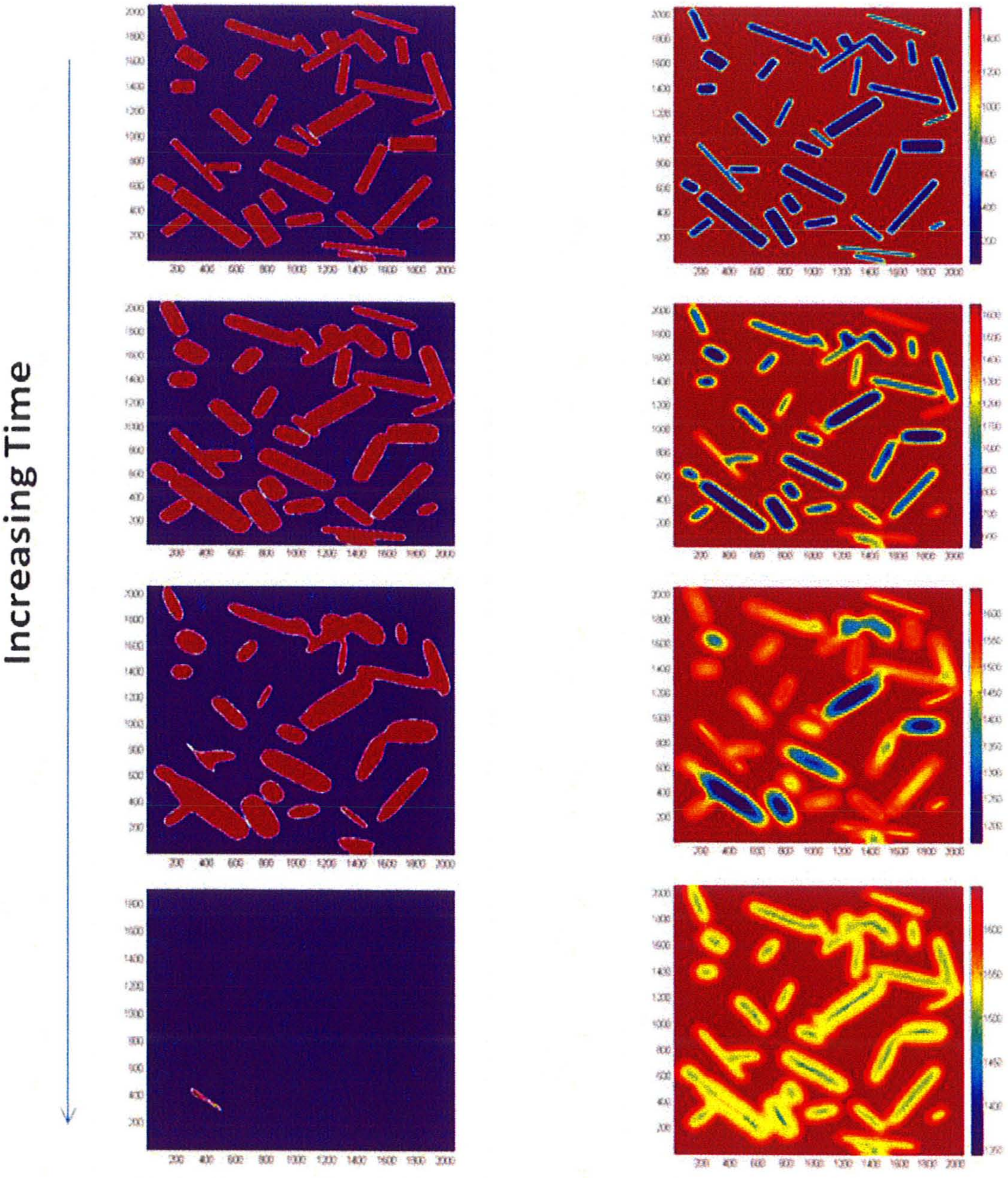

Figure 4-1: A typical melting process of randomly distributed multiple pieces (T_s=298 K, T_L=1873 K, ISF=0.2)

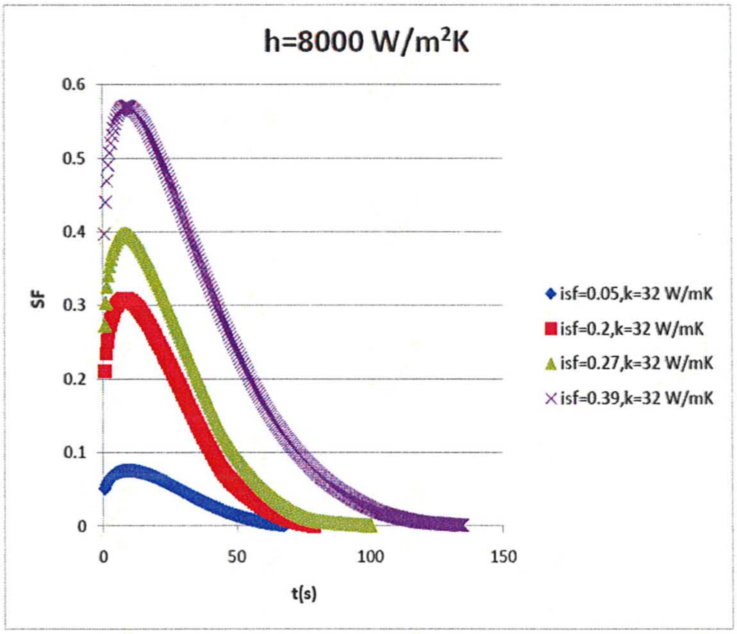

Figure 4-2: The melting profile of scrap pieces having different ISF's but the same heat transfer coefficient (h) of 8000 W/m^{2}K

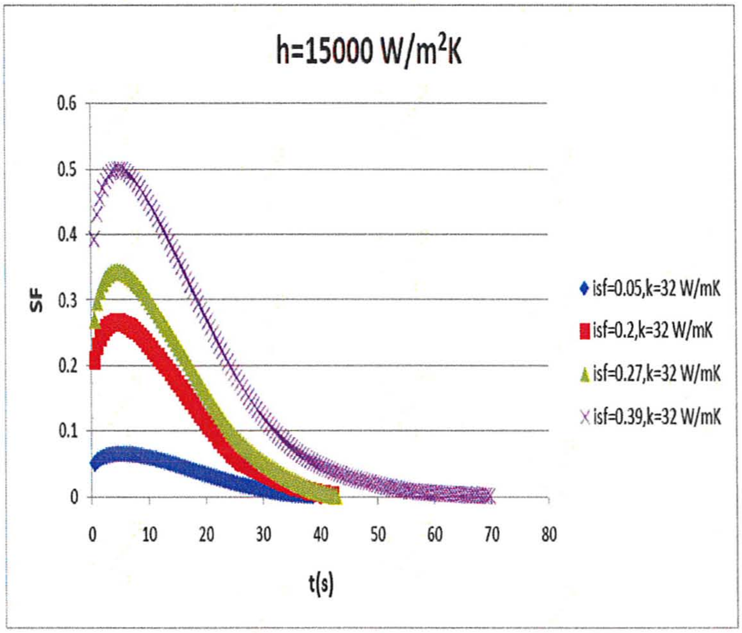

Figure 4-3: The melting profile of scrap pieces having different ISF's but the same heat transfer coefficient (h) of 15000 W/m^{2}K

It is noted that for the cases shown in the Figures 4-2 and 4-3 case, all curves peak at the same time. This suggests that the maximum solid fraction has been reached at the same time for all systems having the same heat transfer coefficient (h) independent from ISF. The time to reach the maximum solid fraction only depends on the heat transfer coefficient (h). It has been also found that the ratio between the maximum solid fraction and the ISF remains constant for systems having the same heat transfer coefficient if the scrap sizes remain constant. This further suggests that the heat transfer coefficient controls the amount of solidification created.

It can also be seen in the data of Figures 4-2 and 4-3 that with decreasing ISF, the plateau period becomes more obvious, while in the systems with larger ISFs, the curves become "sharper". The plateau regions become almost completely flat in single scrap piece, as shown by Li [Li, 2006]. In this case, systems having larger ISFs have larger numbers of scrap pieces and every individual scrap piece begins melting at a different time, the plateau period is not apparent. The curve is essentially averaging over multiple pieces, some of which may already have started melting back while others are just growing or entering the plateau region.

Figure 4-4 shows that the data of Figures 4-2 and 4-3 can each be scaled onto a common function through appropriate choices of time and length scales, represented at this stage heuristically by t_c, SF_c, t_0 and SF_0, respectively. These scaling parameters will be discussed below. The scalability of the curves suggests that, even in systems having different ISFs, melting behavior is universal. It should be noted that the x and y axes are dimensionless after application of the scaling factors.

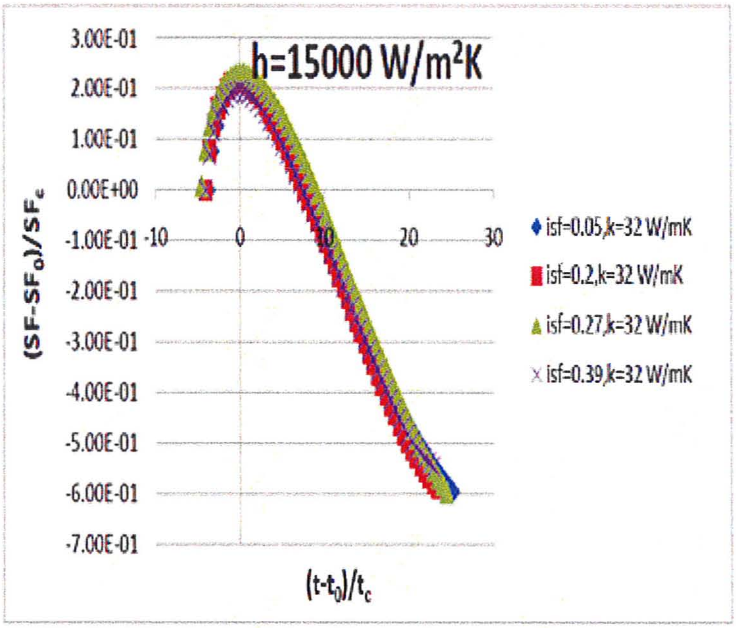

Figure 4-4: The curves in the Figure 4-3 are scaled on a reference curve. The same is true for all heat transfer coefficients.

4.2.2 Effect of Heat Transfer Coefficient (h)

To investigate the effect of the heat transfer coefficient (h) on the system, simulations were performed with four different heat transfer coefficients (5000 W/m^{2}K, 8000 W/m^{2}K, 15000 W/m^{2}K, 20000 W/m^{2}K), in four different systems having four different ISFs (0.05, 0.2, 0.27, 0.39). Thermal conductivities (k), preheating Temperatures (T_s), liquid Temperatures (T_L), and scrap sizes were all kept constant for these cases (k=32 W/m·K, T_s= 298 K, T_L=1923 K scrap size=0.001 m^2).

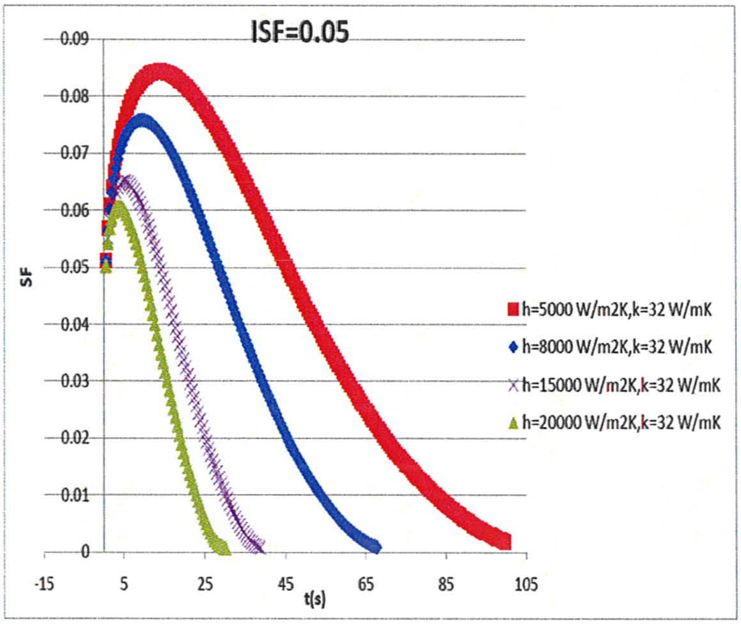

Figure 4-5: The melting profile of scrap pieces having different heat transfer coefficients (h) but the same ISF of 0.05

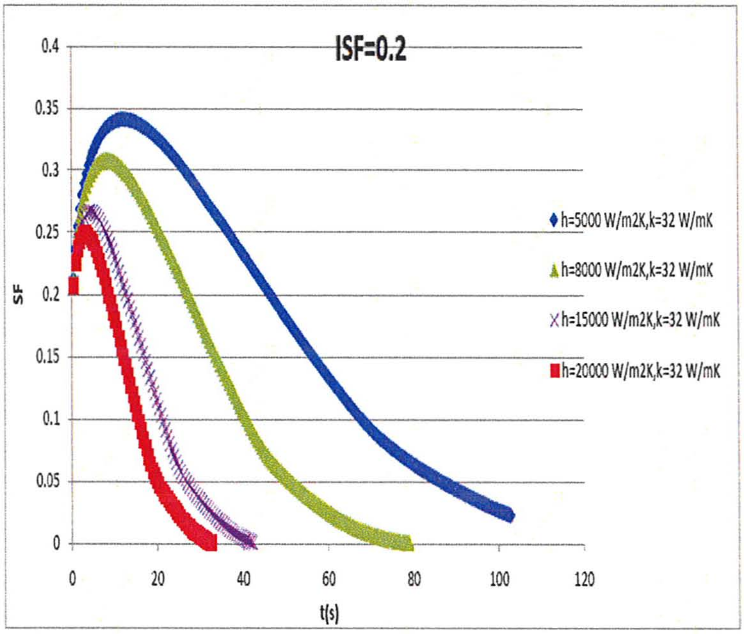

Figure 4-6: The melting profile of scrap pieces having different heat transfer coefficients (h) but the same ISF's of 0.2

In the Figures 4-5 and 4-6, two examples are given to show the typical results of the second part of the investigation. As seen from both figures, the maximum solid fraction, which is represented by the peak of the curve, becomes larger with the decreasing heat transfer coefficient. In contrast with the first investigation discussed above, the time to reach the maximum solid fraction increases as the heat transfer coefficient decreases. This observation also proves the hypothesis presented in the previous section, where the heat transfer coefficient is suggested to control the amount of time needed to reach maximum solidification. The results basically indicate that increasing the amount of stirring of the system, which is represented by the heat transfer coefficient, can reduce the amount of solidification and total melting time. The data in Figures 4-5 and 4-6 can also be described by a scaling formalism, shown in Figure 4-7. As seen from the figure, the curves fit on a reference curve after non-dimensonalization of time and initial solid fractions (i.e. length). The scaling coefficients are denoted with the same symbols as those in Figure 4.4. The unified description of these scaling parameters in terms of all parameters examined in these sub-sections will be presented at the end of this chapter.

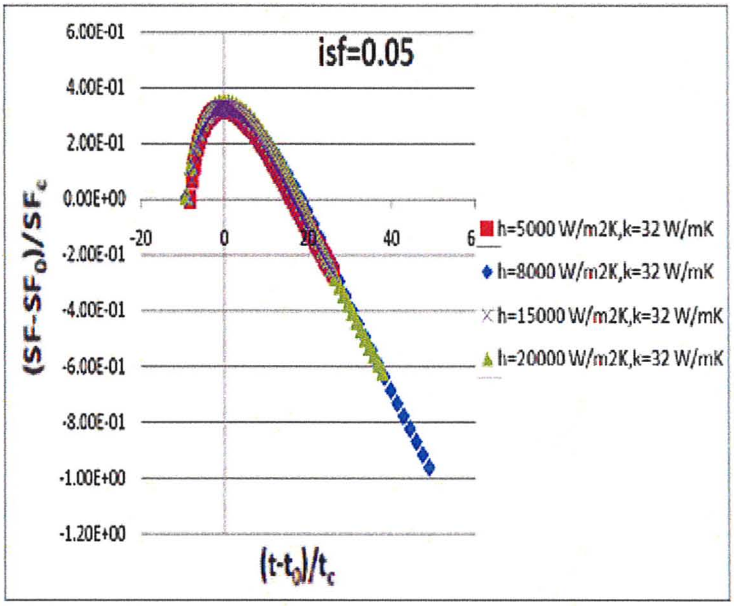

Figure 4-7: Scaling kinetics for systems having different heat transfer coefficients.

4.2.3 Effect of Thermal Conductivity (k)

Melting with different thermal conductivities in the solid (k) was investigated. Variation of k here was chosen to emulate the effect of alloying elements on the melting behavior, but it should be noted that the rest of the materials properties are assumed to be equal to the properties of 1018 solid steel shown in the Table 4-1 and liquid steel shown in the Table 4-2. It is suggested that investigating steel in this way can provide insight into the effect of thermal conductivity on melting behavior. Thermal properties were taken at a temperature 1473K.

To investigate the effect of thermal conductivity (k) on the system, simulations were performed with four different levels of thermal conductivity (26 W/m·K, 32 W/m·K, 40 W/m·K, 48W/m·K), in four systems having different ISF values (0.05, 0.2, 0.27, 0.39). Heat transfer coefficients (h), preheating Temperatures (T_s), liquid Temperatures (T_L), and scrap sizes were kept constant (h=8000 W/m^2·K, T_s= 298 K, T_L=1923 K, scrap size=0.001 m^2).

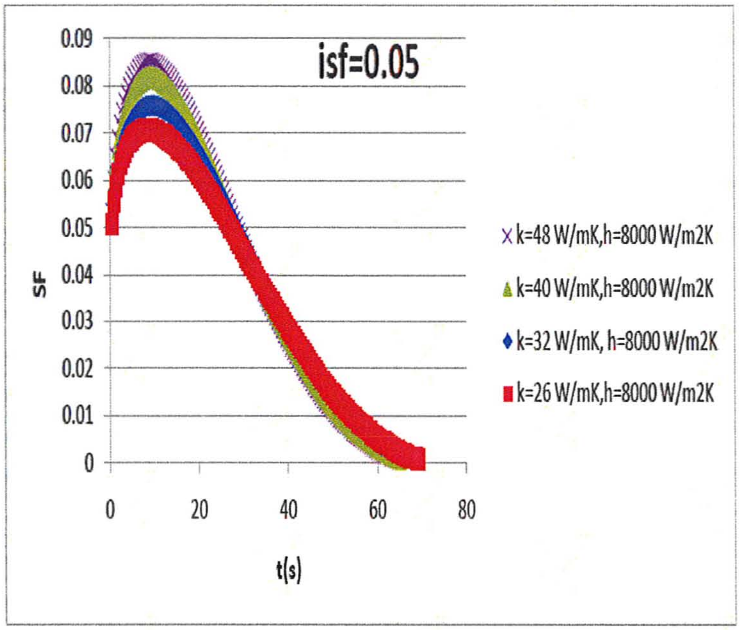

Figure 4-8: The melting profile of scrap pieces having different thermal conductivity(k) levels but the same ISF of 0.05

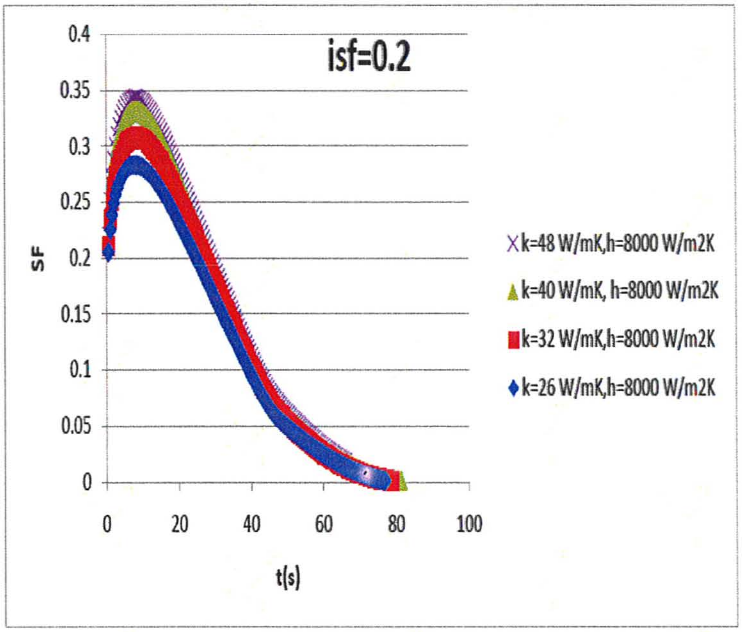

Figure 4-9: The melting profile of scrap pieces having different thermal conductivity (k) levels but the same ISF of 0.2

In figures 4-8 and 4-9, two typical examples can be seen from systems having different thermal conductivities. It can be seen that the amount of solidification is increasing in tandem with thermal conductivity but it does not have a significant effect on the total time. The effect of thermal conductivity on the amount of solidification can be seen more clearly in the Figure 4-10, where only the solidification and remelting stages are shown. Figure 4-11 shows that the data of Figures 4-8 and 4-9 can be scaled onto a reference curve after application of scaling parameters and non-dimensionalization of the time and solid fractions axes.

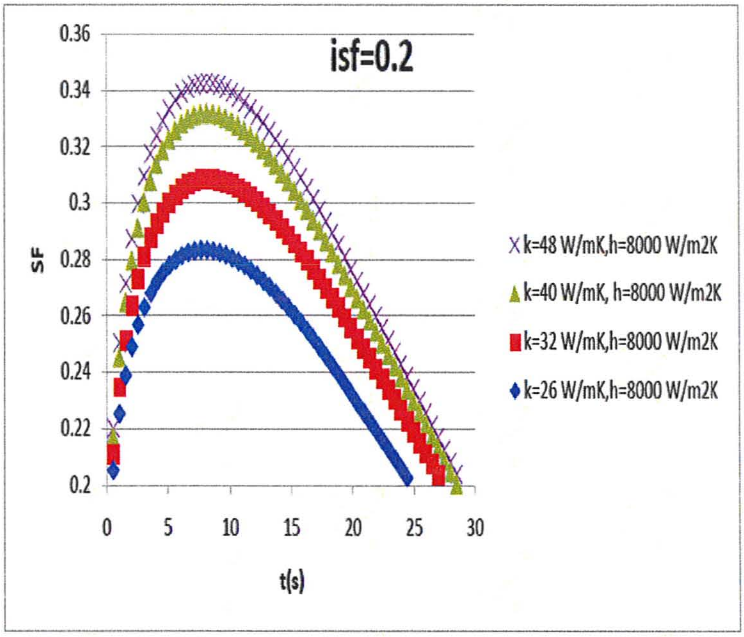

Figure 4-10: A closer look at the effect of thermal conductivity on the amount of solidification.

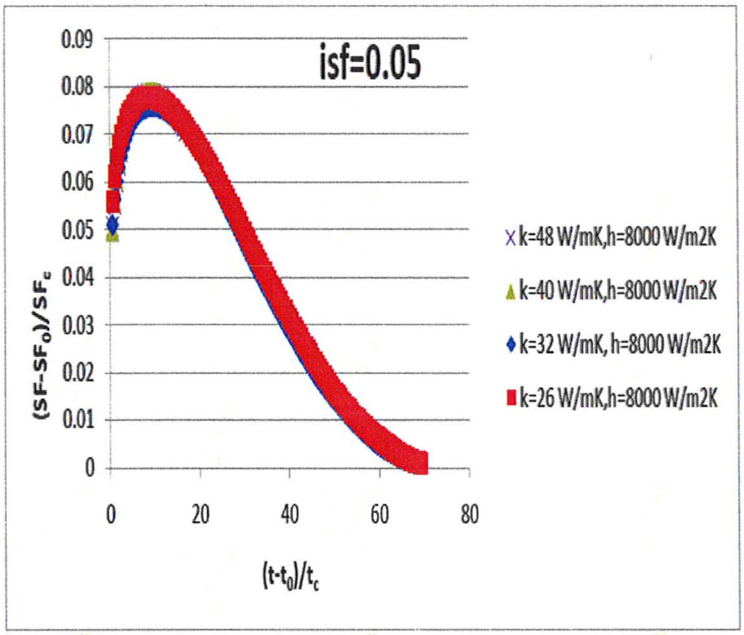

Figure 4-11: Scaling of melting kinetics for systems having different thermal conductivities.

4.2.4 Effect of Liquid Steel Temperature (T_L)

For investigation of the effect of Liquid Steel Temperature (T_L) on the system, simulations were performed with four different temperatures of liquid steel (1923 K, 2000 K, 2100 K, 2200 K) in four different systems having four different ISFs (0.05, 0.2, 0.27, 0.39). Heat transfer coefficients (h), preheating Temperatures (T_s), thermal conductivities (k) and scrap sizes were kept constant (h=20000 $W/m^2 \cdot K$, T_s= 298 K, k= 32 $W/m \cdot K$, scrap size=0.001 m^2).

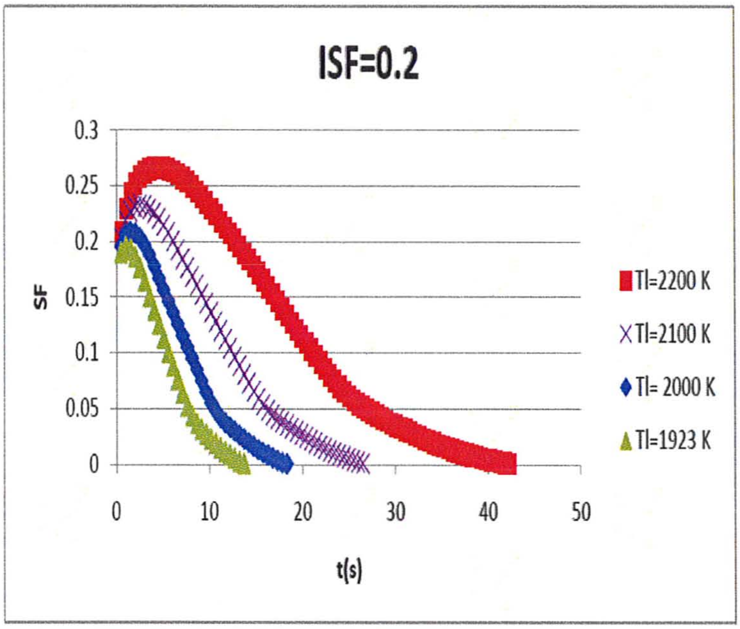

Figure 4-12: The melting profile of scrap pieces having liquid steel temperatures (T_L) but the same Initial Solid Fraction of 0.2

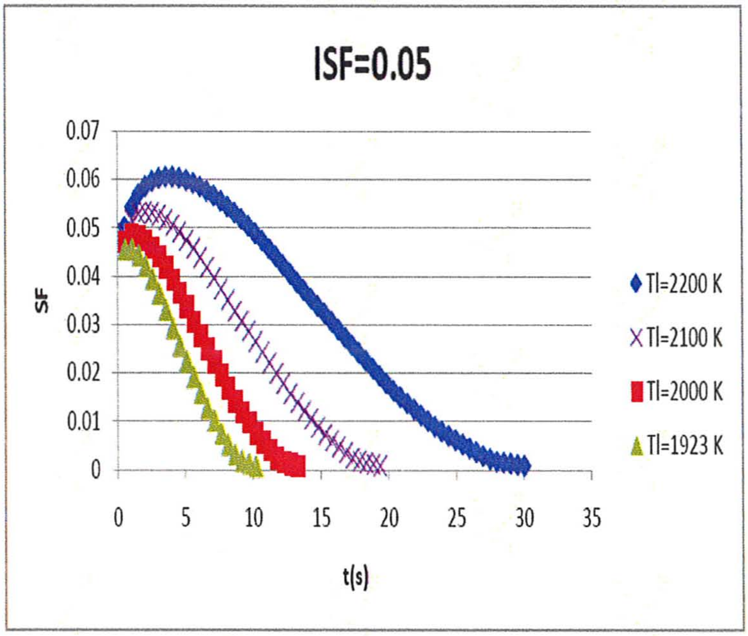

Figure 4-13: The melting profile of scrap pieces having different liquid steel temperatures (T_L) but the same Initial Solid Fraction of 0.05

As seen from Figure 4-12 and 4-13, the amount of solidification and the total melting time increases with increasing undercooling. Considering that the liquid steel temperature actually represents the superheat in this system, this is a very sensible result. It should be noted that although the temperature range is relatively small (1923 K-2200 K), the effect of different liquid steel temperatures on melting time is dramatic. As with the cases discussed above, this data can also be described by a scaling function, as shown in Figure 4-14. As seen, the systems scale very well after non-dimensionalization of the x and y axes.

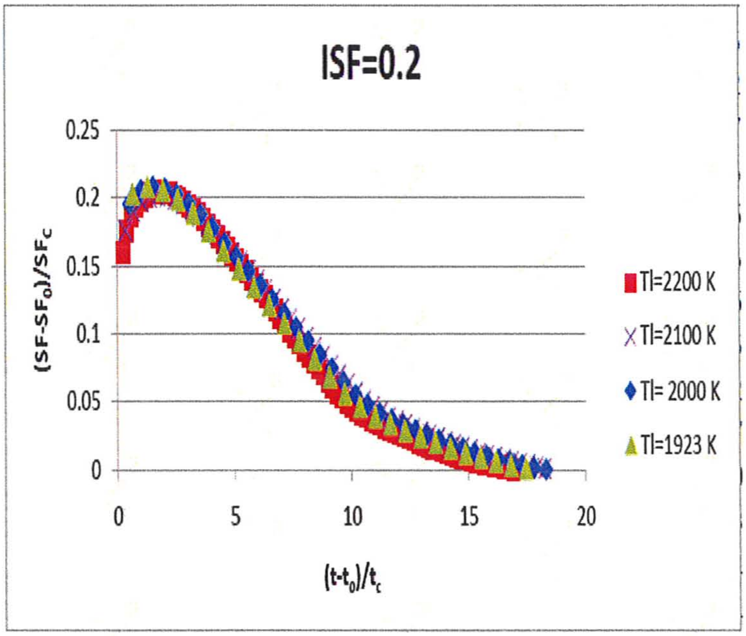

Figure 4-14: Scaling of melting kinetics for systems having different initial liquid temperatures.

4.2.5 The Effect of Preheating Temperature (T_s)

To investigate of the effect of Preheating Temperature (T_s) on the system, simulations were performed with four different temperatures of initial scrap temperature (298 K, 400 K, 600 K, 800 K) in four different systems having different ISFs (0.05, 0.2, 0.27, 0.39). Heat transfer coefficients (h), liquid steel temperature (T_L) thermal conductivities (k) and scrap sizes were kept constant (h=20000 $W/m^2 \cdot K$, T_L = 1923 K, k= 32 W/m·K, scrap size=0.001 m^2).

As seen in Figures 4-15 and 4-16, the amount of solidification and the total melting time increase as preheating temperature decreases. Also, it should be noted that, although the temperature range is much larger (298 K-800 K), than the liquid steel temperature range, the effect of variation of preheating temperature on total melting time has much less of an effect than the effect of liquid steel temperature. A scaling analysis for these systems is shown in Figure 4-17. As seen, the systems scale very well after non-dimensionalization of the x and y axes.

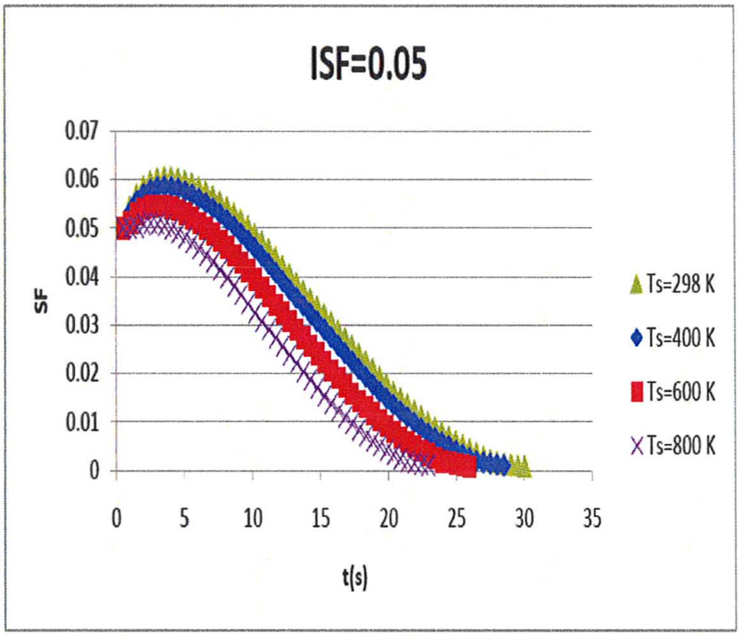

Figure 4-15: The melting profile of scrap pieces having different preheating temperatures (T_s) but the same Initial Solid Fraction of 0.05

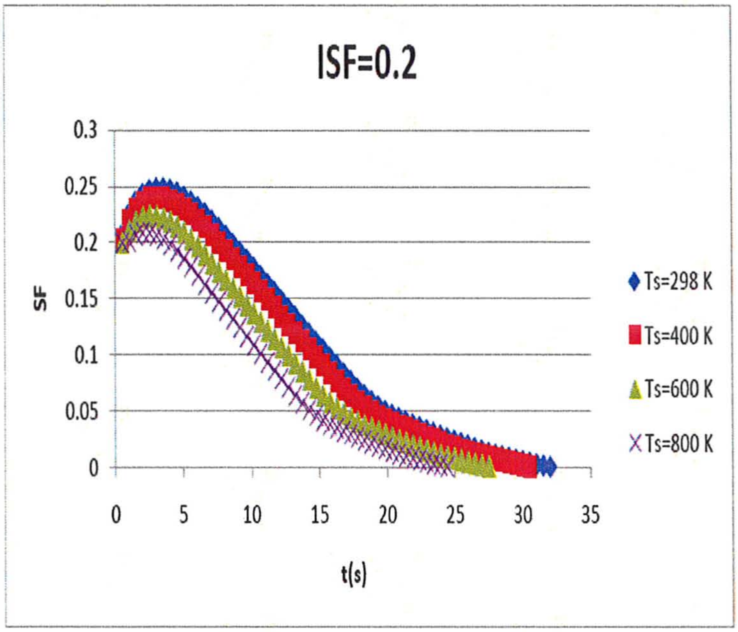

Figure 4-16: The melting profile of scrap pieces having different preheating temperatures (T_s) but the same Initial Solid Fraction of 0.2

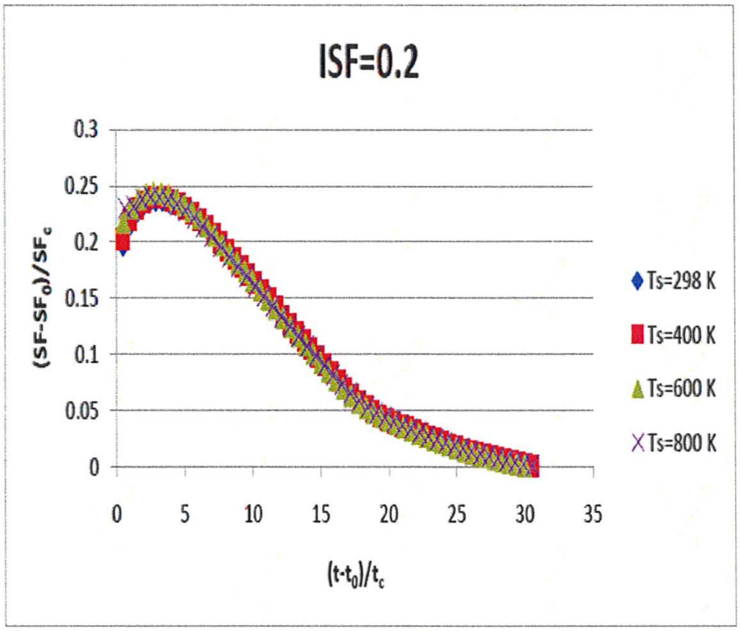

Figure 4-17: Scaling analyses for systems having different preheating temperatures.

4.2.6 Effect of Scrap Size

In this section, the sizes of the rectangular shaped scrap pieces are changed by changing both the width and the length of the pieces. For investigation of the effect of scrap size on the system, simulations were performed with four different scrap sizes (0.001 m^2, 0.00144 m^2, 0.00188 m^2, 0.002 m^2) in four systems having different heat transfer coefficients (5000 W/m^2K, 8000 W/m^2K, 15000 W/m^2K, 20000 W/m^2K). Liquid steel temperature (T_L), preheating Temperature (T_s) and thermal conductivities (k) (T_L = 1923 K, T_S=298 K, k= 32 W/m·K) were kept the same for these systems. It should be mentioned that the ISF, which is calculated with the equation in 4.1, was not kept constant; instead, the number of scrap pieces put in the system has been changed.

As seen from Figure 4-18 and 4-19, the amount of solidification and the total melting time increase with increasing preheating scrap size. Also, the curves show parallel behavior and they have the same shapes, suggesting, as in all previous cases, that the different curved can be scaled onto a common curve, as shown in Figure 4-20.

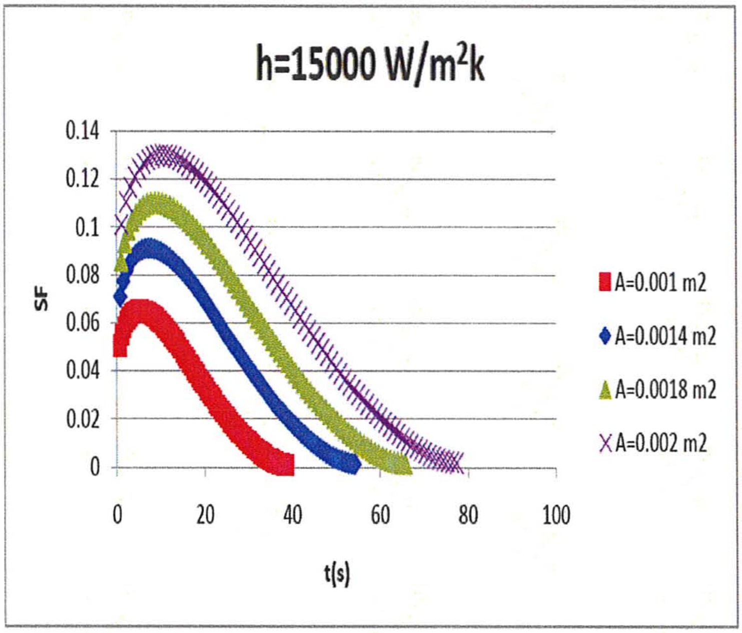

Figure 4-18: The melting profile of scrap pieces having different scrap sizes, but the same heat transfer coefficient (15000 W/m^2)

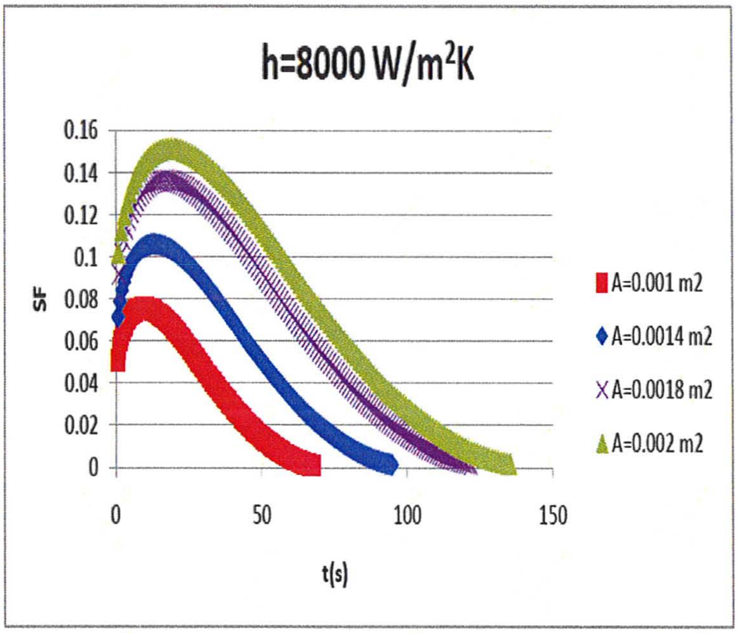

Figure 4-19: The melting profile of scrap pieces having different scrap sizes, but the same heat transfer coefficient (8000 W/m^2)

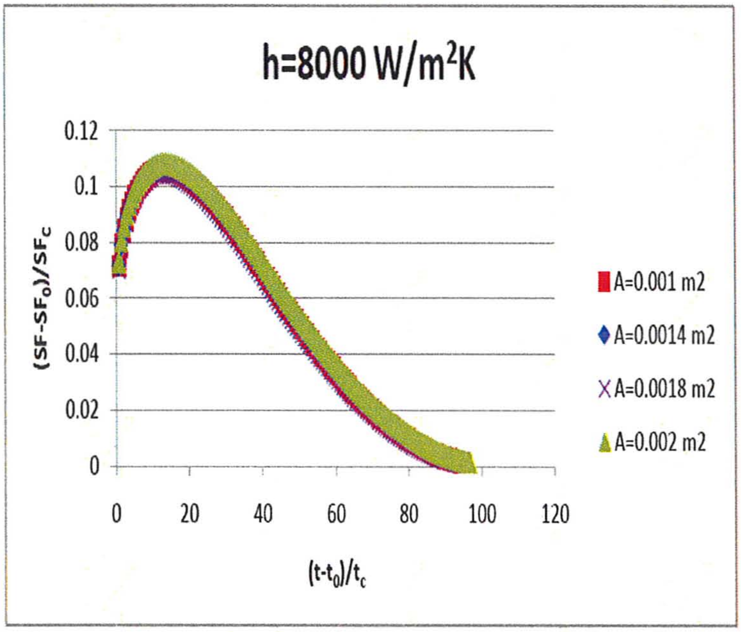

Figure 4-20: Scaling analysis for the systems having different scrap sizes

4.3 Scaling Laws as a Tool in Materials Science

Scaling is technique based on non-dimensionalization of governing equations and variables where non-dimensional groups can express the overall behavior of the whole system. Obtaining a scaling law to explain a process is a great tool for engineers and scientists since it allows them to obtain universal behavior of certain scientific phenomenon. Extrapolating general behavior makes it possible to extract results for specific cases faster and easier, without performing experiments or running simulations.

Non-dimensionalization of a phenomenon can result in three different scenarios depending on the initial problem [Irons *et al.*, 2010]:

1. Complete physical understanding and mathematical expressions based on obtaining of differential equations and constitutive relations
2. Partial physical understanding of possible mechanisms and ratios
3. No real physical understanding of the process but insight into the effect of the input parameters. Third scenario is also called Dimensional Analysis.

The first known attempt of a scaling analysis was done by Fourier in 1822 in the area of heat transfer. In 1914 E. Buckingham came up with the "Buckingham Pi Theorem". Buckingham's Pi Theorem basically suggests that, if a system contains M variables and these variables contain N dimensions, the number of non-dimensionless groups should be {M-N}. These groups are referred as "π" groups. π groups should be independent from each other and their products should not create new non-dimensional groups. Since the invention of Buckingham Pi Theorem, scaling has been commonly used in fluid mechanics, transport phenomena and heat transfer. Scaling laws presented in several transport phenomena books written by Geankopolis [Geankopolis, 2003], Bird *et al.* [Bird *et al.,* 1960] and Szekely *et al.* [Szekely *et al.,* 1971].

As an example, Szekely *et. al.* [Szekely *et al.,* 1971] in their work studied scaling in heat transfer in a steel slab having thickness of L and initial temperature of T_i. The temperature of the surroundings denoted T_e. This problem can be formulated as

$$\frac{\partial T}{\partial t} = \frac{K}{c\rho}\frac{\partial^2 T}{\partial X^2} \qquad 0 \leq X \leq L \qquad (4.2)$$

with

$$T = T_i \qquad \text{at } t=0 \qquad (4.3)$$

and

$$-K\frac{\partial T}{\partial X} = \varepsilon\sigma\left(T^4 - T_e^4\right) \qquad \text{at } X=0 \text{ and } X=L \qquad (4.4)$$

The following dimensionless parameters are introduced.

Dimensionless Length: $\beta = \frac{X}{L}$ (4.5)

Dimensionless Time (Fourier Number): $\tau = \frac{t\alpha}{L^2}$ (4.6)

where:

$$\alpha = \frac{k}{\rho c} \qquad (4.7)$$

Dimensionless Temperature: $T_d = \dfrac{T}{T_i}$ (4.8)

In terms of these dimensionless variables, Equation 4.1 becomes:

$$\frac{\partial T_d}{\partial \tau} = \frac{\partial^2 T_d}{\partial \beta^2} \qquad 0 \leq \beta \leq 1 \qquad (4.9)$$

The time required to reach steady state can be calculated by putting

$$\tau = \frac{t\alpha}{L^2} \sim 1$$

which will result in

$$t \approx \frac{L^2}{\alpha}$$

Another example that can be analyzed in terms of a scaling analysis can be given from diffusion where the concentrations of impurities in a material subject to boundary conditions maintaining a concentration C_0 on the surface is given by:

$$C(x, t) = C_0 \operatorname{erfc}\left(\frac{x}{2\sqrt{Dt}} \right) \qquad (4.10)$$

The concentration can be non- dimensionalized using:

Dimensionless concentration: $$C_d = \frac{C}{C_0} \qquad (4.11)$$

and distance can be non- dimensionalized as:

Dimensionless distance: $$x_d = \frac{x}{2\sqrt{Dt}} \qquad (4.12)$$

In terms of these dimensionless variable the curves depicted by Equation 4.10, shown in the left frame of Figure 4-21, are seen to be "stretched" versions of the curve in the right side frame of Figure 4-21.

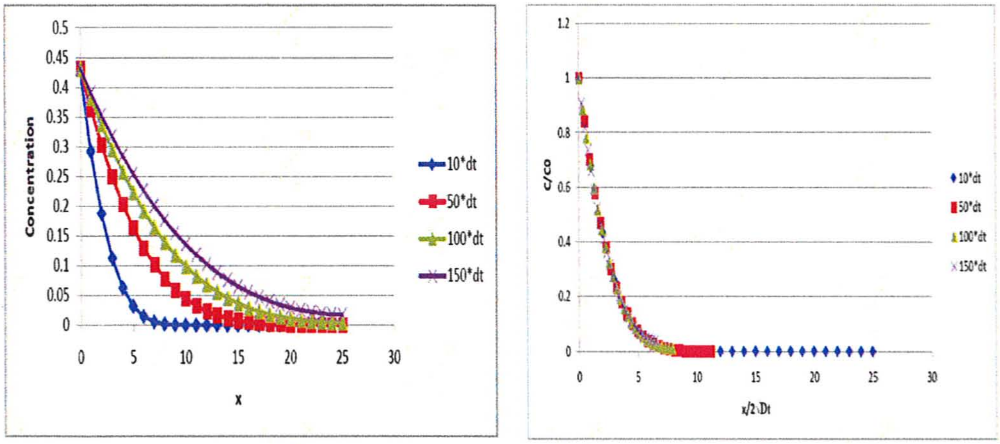

Figure 4-21: Non- dimensionalization of the diffusion problem

Recently, with increasing popularity in the scaling approach, chapters and even entire books are dedicated to use of scaling in heat transfer and transport phenomena. The authors include but are not limited to Denn *et al.* [Denn *et al.,* 1980], Deen *et al.* [Deen *et al,* 1998] and Kline *et al.* [Kline *et al.*, 1986]. Experimental approaches are done by Sides [Sides, 2002], Chen [Chen, 1990] and Astarita [Astarita, 1997]. Scaling techniques are also used in other areas of materials science and engineering, for example, Cebon *et al.* [Cebon *et al.*] suggested using non-dimensionless groups to have a better understanding on the relationships between materials properties and data estimation. Geller *et al.* [Geller *et al.,* 2005] proposed to use a Rice-Thompson parameter as a principle in ductilizing of molybdenum alloys and Dantzig *et al.* [Dantzig *et al.,* 2001] suggested the use of scaling in modeling of materials processing. Most recently, Krantz *et al.* [Krantz *et al.,* 2007] dedicated a book on scaling analysis in transport and reaction process modeling.

4.4 Analyses on Scaling Factors

This section derives predictions for the scaling factors used in the scaling analyses of our scrap melting simulations above.

4.4.1 Calculation of $\frac{SF_{\max}}{ISF}$

Section 4.2.1 noted that the ratio between the maximum solid fraction $SF_{\max}$ and the ISF remains constant for systems having the same heat transfer coefficient. This ratio is denoted by β, and is approximated theoretically as follows:

Solid fraction can be formulated as:

$$SF = \frac{NA}{L_s^2}$$

Also it can easily be seen that:

$$\beta = \frac{SF_{\max}}{ISF} = \frac{A_{\max}}{A_{ini}} \tag{4.13}$$

Defining the following variables,

SF_{max}= Maximum solid fraction

ISF= Initial Solid Fraction

L_{inc}= Increase in the length of an average piece

A_{ini}= Initial area of an average piece=L·w

A_{max}= Maximum area of an average piece

A_{max}= $(L+L_{inc})\cdot(w+L_{inc})$ [assuming that $L_{inc}= w_{inc}$]

A_{max}= $Lw+(L+w)L_{inc}+L_{inc}^{2}$ (4.14)

gives:

$$\beta = \frac{SF_{\max}}{ISF} = \frac{A_{\max}}{A_{ini}} = \frac{Lw+(L+w)L_{inc}+L_{inc}^{2}}{Lw} \tag{4.15}$$

or

$$\beta = \frac{SF_{\max}}{ISF} = 1+\frac{L+w}{w}\frac{L_{inc}}{L}+\frac{L_{inc}^{2}}{Lw} \tag{4.16}$$

Neglecting $\frac{L_{inc}^{2}}{Lw}$ term gives, to lowest order,

$$\beta = \frac{SF_{\max}}{ISF} = 1+\frac{L+w}{w}\frac{L_{inc}}{L} \tag{4.17}$$

We denote;

$$\frac{L_{inc}}{L} = \Delta_{eff} \tag{4.18}$$

where Δ_{eff} is the Effective Growth Ratio

Thus,

$$\frac{SF_{\max}}{ISF} = 1 + \frac{L+w}{w}\Delta_{eff} \tag{4.19}$$

4.4.2 Calculation of Δ_{eff}

For the calculation of Δ_{eff} , the interface heat balance has been used:

$$h(T_L - T_M) = \rho \Delta H_f V - k\left.\frac{\partial T_s}{\partial x}\right|_{\text{int}}$$

When the solidified shell reaches its maximum thickness the velocity becomes zero and the following statement can be made:

$$h(T_L - T_M) = k\frac{(T_M - T_s)}{L^*} \tag{4.20}$$

where

$$\rho HV = 0$$

and

L* = Effective change of the length of the solidified shell around a scrap piece.

It is suggested to use the following formula to equivalently express the growth ratio:

$$\Delta_{eff} = L^{*} \frac{w}{L^{2}} \tag{4.21 a}$$

using Equation 4.20

$$\Delta_{eff} = \frac{k(T_M - T_s)}{h(T_L - T_M)} \frac{w}{L^2} = \frac{L_{inc}}{L} \tag{4.21 b}$$

where $\frac{w}{L}$ is the ratio between the width and length of an average piece.

Equation 4.21 b can be simplified to:

$$\Delta_{eff} = \frac{k(T_M - T_s)}{h(T_L - T_M)} \frac{w}{L^2} = \frac{L_{inc}}{L} \tag{4.22}$$

giving,

$$\beta = \frac{SF_{\max}}{ISF} = 1 + \left[\frac{L + w}{w}\right]\left[\frac{k(T_M - T_s)}{h(T_L - T_M)} \frac{w}{L^2}\right] \tag{4.23}$$

4.4.3 Solid Fraction Scaling Factors

After investigation, we found that the solid fraction axis of our melting versus time plots from our simulation data can be scaled with the following equation:

$$Y_{scale} = \frac{\dfrac{(SF - SF_0)}{SF_0}}{\beta \Delta T_L \Delta T_S \sqrt{\dfrac{H}{K}}} \tag{4.24}$$

where:

$$SF_0 = ISF \tag{4.25}$$

And

$$SF_c = ISF \beta \Delta T_L \Delta T_S \sqrt{\frac{H}{K}} \tag{4.26}$$

$$H = \frac{h_{ref}}{h}$$

$$\Delta T_s = \frac{T_M - T_s}{T_M - T_s^{ref}}$$

$$\Delta T_L = \frac{T_L - T_M}{T_L^{ref} - T_M}$$

$$K = \frac{k_{ref}}{k}$$

where the subscript "ref" refers to a reference curve against which all other curves are scaled. (This can be any of melting curve, which would then simply form a reference).

Equations in 4.25 and 4.26 thus become:

$$SF_o = ISF \qquad (4.27)$$

and

$$SF_c = ISF\left(1+\frac{L+w}{L^2}\right)\left(\frac{k}{h}\right)^{3/2}\left(\frac{h_{ref}}{k_{ref}}\right)^{1/2}\left(\frac{(T_M - T_S)^2}{\left(T_M - T_s^{ref}\right)\left(T_L^{ref} - T_M\right)}\right) \qquad (4.28)$$

4.4.4 Calculation of Scaling Factors of Time Scale

After investigations, it was found that the time axis in our melting curves can be scaled according to the form:

$$X_{scale} = \frac{t-(t_{eff}\frac{H}{L^{\alpha}})}{t_{eff}\frac{H^2}{L^{\alpha}}\Delta T_L^2 \Delta T_S^2} = \frac{t-t_0}{t_c} \qquad (4.29)$$

where:

$$L^{\alpha} = \frac{L_{ref}}{L} \qquad (4.30)$$

$$t_0 = t_{eff}\frac{H}{L^{\alpha}} \qquad (4.31)$$

$$t_c = t_{eff}\frac{H^2}{L^{\alpha}}\Delta T_L^2 \Delta T_S^2 \qquad (4.32)$$

To calculate the effective time, the interface heat balance is used again:

$$h(T_L - T_M) = \rho \Delta H_f V - k \left.\frac{\partial T_s}{\partial x}\right|_{\mathrm{int}}$$

The velocity of the interface can be calculated as:

$$V = \frac{dL_{inc}}{dt_{eff}} = \frac{h(T_L - T_M)}{\rho \Delta H_f} - \frac{k}{\rho \Delta H_f} \frac{(T_M - T_s)}{L_{inc}(t)} \qquad (4.33)$$

Integrating Equation 4.33 gives,

$$t_{eff} = \frac{L_{inc}}{\frac{h(T_L - T_M)}{\rho \Delta H_f}} \qquad (4.34)$$

If we rearrange the terms in Equations 4.31 and 4.32 gives:

$$t_o = \rho \Delta H_f \frac{h_{ref} k}{h^3} \frac{w}{L_{ref}} \frac{(T_M - T_s)}{(T_L - T_M)^2} \qquad (4.35)$$

and

$$t_c = \rho \Delta H_f \frac{h_{ref}{}^2 k}{h^4} \frac{w}{L_{ref}} \frac{(T_M - T_s)^3}{\left(T_l^{ref} - T_M\right)^2 \left(T_M - T_s^{ref}\right)^2} \qquad (4.36)$$

4.5 Unified Scaling Analysis of all Data

Figure 4-21 shows the scaling of all simulated data presented in this chapter using the theoretically predicted scaling factors derived in Section 4.2 for SF_c, SF_0, t_0, t_c (i.e. Equations 4.27, 4.28, 4.35, 4.36). It is noted that only data in the linear regime of all melting curves is shown, for the model is expected to break down for later times, as explained above.

Figure 4-22 shows the scaling of all the data using the heuristically determined (i.e. fit manually to obtain the best alignment of the data) scaling factors for SF_c, SF_0, t_0, t_c. The theoretical scaling factors applied in Figure 4-21 and empirically fitted scaling factors used to scale the curves as shown in the Figure 4-22 show a small amount of difference. This is due to the fact that the theory presented here is approximate. Moreover, the heuristically fit data also carries an error as it was done by visual inspection. A comparison of theoretical and fit scaling coefficients is shown in Figure 4-23. In this figure, the scaling factors shown are for systems having different ISFs but the same heat transfer coefficients, thermal conductivities, liquid and preheating temperatures, and scrap sizes has been compared. As seen in the Figure 4-23, the scaling factors predicted theoretically and fit heuristically are in fairly good agreement.

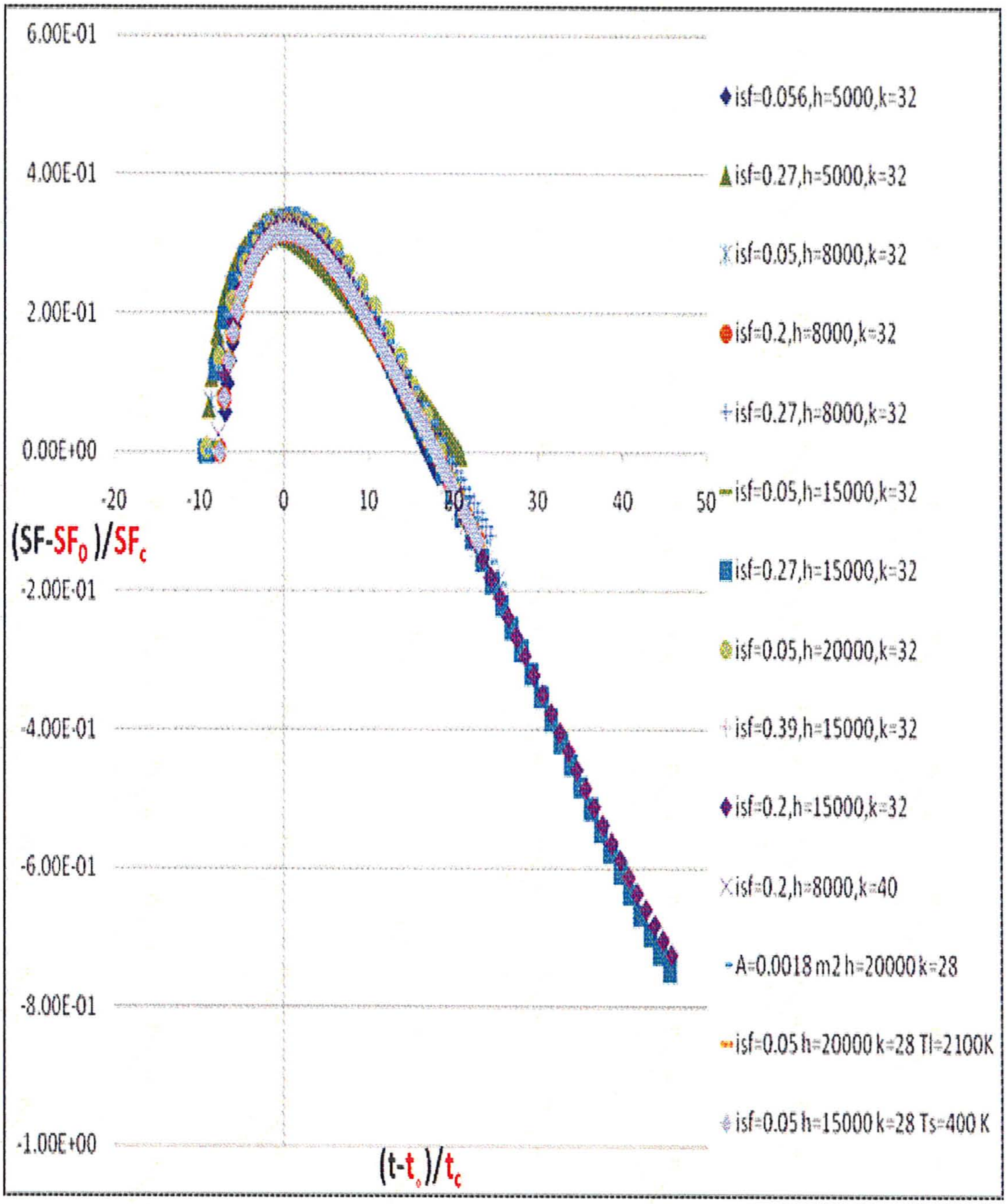

Figure 4-22: Universal scaling of all simulation data using theoretically predicted scaling factors.

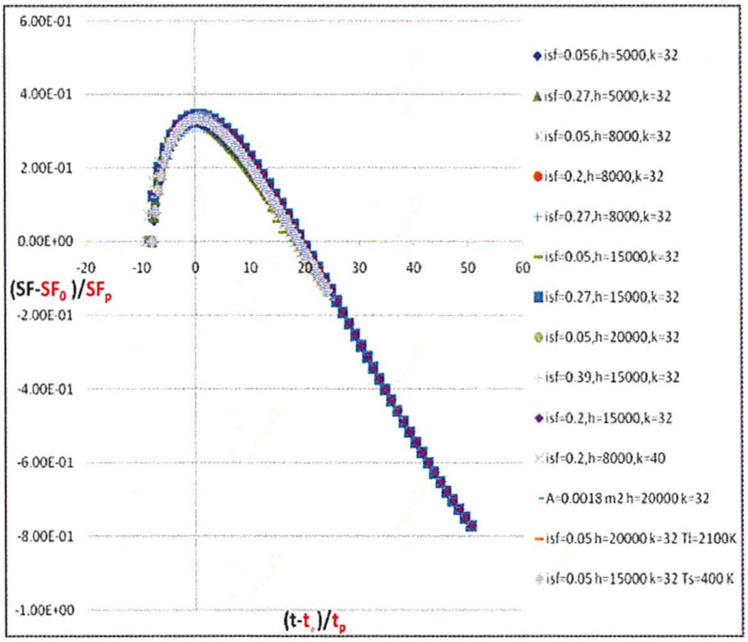

Figure 4-23: Curves scaled with empirically fitted scaling factors

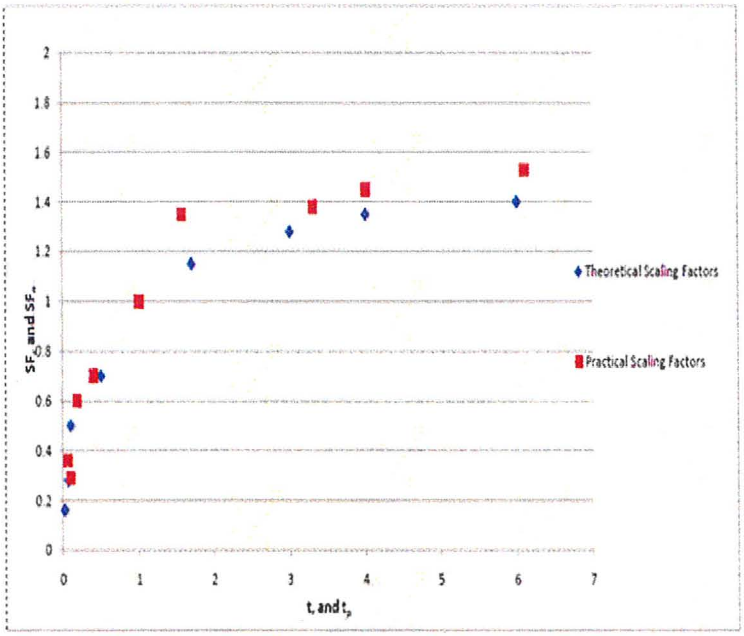

Figure 4-24: Practical versus theoretical scaling factors

Chapter 5
Summary and Conclusions

This work studied simulations of melting of randomly distributed multiple steel scrap pieces. The model used was that previously developed by Li [Li, 2006]. The aim of this study was to better understand the universal features governing the kinetics of multi-piece scrap melting in a liquid pool. The key observations regarding the conditions melting for a single scrap piece are summarized below:

(1) After immersing the cold scrap piece into a hot liquid bath, a solidified shell is formed.

(2) There is an interfacial gap between the original bath and solidified shell. This gap is caused by the imperfect contact between solid and liquid.

(3) The interfacial gap sucks buffers heat moving through the solidified shell and stalls the growth of the solidified shell. This discontinuation of the solidified shell formation is represented as the "plateau period" in plots of bar size versus time.

(4) To model the heat transfer throughout the interfacial gap, a model of the strip casting has been used [Li, 1996] for the heat conductivity in the gap region. According to the model, the phenomenological effective thermal conductivity (k_{eff}) is defined in in the interfacial gap, changing in time according to the form, $k_{eff}= k_0(1+t)^m$

(5) Scrap pieces agglomerate because of the solidified shell formation. These agglomerated pieces are referred as "steel icebergs", should also include the properties of the scrap, number, type of distribution, geometry, etc.

The following summarize the main conclusions about the melting kinetics of randomly distributed scrap pieces made in this thesis.

(1) The maximum solid fraction to initial solid fraction ratio remains constant if the average scrap size is kept constant for the systems having the same heat transfer coefficient (h). This ratio is referred as β and defined as $\beta=1+\frac{L+w}{w}\frac{L_{inc}}{L}$

(2) The larger the scrap size, the longer the total melting time and the maximum solid fraction. β increases along with scrap size since the larger scrap pieces create larger steel icebergs.

(3) Melting time data for multi-piece distributions were obtained under different process and parameter conditions. The data was subjected to a multi-parameter scaling analysis in order to collapse the different melting curves onto a so-called universal theory where each melting heat is distinguished by a characteristic length and time. The latter are referred to as "scaling factors". The following summarizes the scaling factors that were formulated to obtain scaling collapse of the scrap melting data in a liquid pool:

a. The Y axis is represented in dimensionless form according to the formula:

$$Y_{scale} = \frac{SF - SF_0}{SF_c}$$

where

$$SF_o = ISF$$

and

$$SF_c = ISF\left(1 + \frac{L + w}{L^2}\right)\left(\frac{k}{h}\right)^{3/2}\left(\frac{h_{ref}}{k_{ref}}\right)^{1/2}\left(\frac{(T_M - T_S)^2}{(T_M - T_s^{ref})(T_l^{ref} - T_M)}\right)$$

b. The X axis is cast into dimensionless form according to the formula

$$X_{scale} = \frac{t - t_0}{t_c}$$

where

$$t_o = \rho \Delta H_f \frac{h_{ref} k}{h^3} \frac{w}{L_{ref}} \frac{(T_M - T_s)}{(T_L - T_M)^2}$$

and

$$t_c = \rho \Delta H_f \frac{h_{ref}^{\,2} k}{h^4} \frac{w}{L_{ref}} \frac{(T_M - T_s)^3}{(T_l^{ref} - T_M)^2 (T_M - T_s^{ref})^2}$$

It is noted that the above scaling factors are given in terms of materials and process parameters that are know or can be in principle measured. It would be instructive in the sequel to re-express these scaling factors in terms of the more standard dimensionless groups used in the steel processing literature.

BIBLIOGRAPHY

Adolph, H., Paul, G. and Klein K. H. (1989)." A New Concept for Using Oxy-Fuel Burners and Oxygen Lances to Optimize Electric Arc Furnace Operation." Electric Furnace Conference, Vol. 46; Pittsburgh, Pennsylvania; USA., 251-257

Astarita, G. (1997). "Dimensional Analysis, Scaling, and Orders of Magnitude." Chemical Engineering Science, 52(24), 4681-4698.

Baukal, C. E., Lanyi, M. D and Winchester, D. C. (1990). "Scrap Preheating With a Submerged Oxygen-Fuel Burner." Iron & Steelmaker, Vol 17, No 10, 51-56.

Bird, B. R., Steward, W. E., Lightfoot, E. N. (1960). Transport Phenomena 1st Edition, New York, USA, John Wiley & Sons.

Brabie, L. C., Kawakami, M. (2000). "Kinetics of steel scrap melting in molten Fe-C bath." High Temperature Materials and Processes, 19: 241-255.

Picture of scrap pieces with different shapes and sizes. Retrieved Aug. 2, 2010 from http://www.caltechcorp.com/8.html. Caltech International Trading Corporation, New York, NY.

http://www.canadiansteel.ca. Canadian Steel Producers Association, Ottawa, ON. Retrived Aug. 1, 2010.

Cebon, D., Ashby, M. F. (2006). "Engineering Materials Informatics." MRS Bulletin, 31(12).

Chen, M. M. (1990). "Scales, Similitude, and Asymptotic Considerations in Convective Heat Transfer." Annual Review of Heat Transfer, 233-391.

Dantzig, J. A., Tucker, C. L. (2001). Modeling in Materials Processing. Cambridge, UK, Cambridge University Press.

Deen, W. M. (1998). Analysis of Transport Phenomena. NY, USA, Oxford University Press.

Denn, M. M. (1980). Process Fluid Mechanics 1st Edition. NJ, USA, Prentice Hall Press.

Franklin, J. (1991). "Scrap preheating at Harrison Steel Casting Company." Iron & Steelmaker, Vol 18, No 5, 57-58.

Fruehan, R. J. (1985). The Making, Shaping and Treating of steel: Steelmaking Volume, 10th Edition. Pittsburgh, PA, USA, AISE Steel Foundation.

Gaye, H., Wanin, M.m Guglerma, P., Schittly, P. (1985). "Kinetics of scrap dissolution in the converter." Proceeding of the 6th Steelmaking Conference, Detroit, USA, ISS: 793-806.

Geankoplis, C. J. (2003). Transport Processes and Separation Process Principles 4th Edition. NJ, USA, Prentice Hall Press.

Geller, C. B. (2005). "A Computational Search for Ductilization Additives to Mo." Scripta Materialia, 52 (3), 205-210.

Gripenberg, H., Brunner, M. (1990). "Optimal distribution of oxygen in high efficiency arc furnaces." Iron and Steel Engineer, 67(7); 33-37.

Guthrie, R. I. L., Gourtsoyannis, L. (1971). "Melting rates of furnace or ladle additions in steelmaking." Canadian Metallurgical Quarterly, 10(1); 37-46.

Incorpera, F. P., Dewitt, D. P. (2002). Fundamentals of Heat and Mass Transfer 5th Edition. New York, USA, John Wiley & Sons Press.

Irons, G.A., Krishaposhoridy, K. (2010). Physical and Mathematical Modeling course notes: McMaster University, Department of Materials Science & Engineering, Hamilton, ON .

Kawai Y., Shiraishi Y. (1998) Handbook of Physico-Chemical Properties at High Temperatures, Tokyo, Japan, ISIJ: 35-123.

Kim, Y. U., Pehlke, R. D. (1974). "Mass transfer during dissolution of a solid into liquid in the carbon-iron system." Metallurgical Transactions, 5(12): 2527-2532.

Kline, S. J. (1986). Similitude and Approximation Theory. NY, USA, Springer.

Kosaka, M., Minova, S. (1967). Tetsu-to-Hagane, 53; 983.

Krantz, W. B. (2007). Scaling Analysis in Modeling Transport and Reaction Processes: A Systematic Approach to Model Building and the Art of Approximation. New York, USA, John Wiley & Sons Press.

Lampman Ed., S. R., (1990). *Metals Handbook: Properties and Selections: Iron and Steel.* Materials park, OH, USA, ASM.

Landau, R .H., Paez, M. J. (1997) Computational Physics: Problem Solving with Computers. New York, USA, John Wiley & Sons.

Li, G., Thomas. B. G. (1996). "Transient Thermal Model of the Continous Single-Wheel Thin-Strip Casting Process." Metallurgical and Materials Transactions B, 27B(3): 509-525.

Li, J. (2006). Kinetics of Steel Scrap Melting in Liquid Steel Bath in an Electric Arc Furnace (PhD Thesis). Department of Materials Science and Engineering, McMaster University, Hamilton, ON.

Li, Y., Fruehan, R. J. (2003). "Computation Fluid-Dynamics Simulation of Postcombustion in the Electric Arc Furnace." Met Trans B, Vol 34B, 333-343.

Lommel, J. M., Chalmers, B. (1959) "The Isothermal Transfer From Solid to Liquid in Metal Systems", AIME Trans, Vol 215, 499-508.

Mandal, K., Irons, G. A. (2005). Private communication between Dr. Jianghua Li and Kamalesh Mandal, Department of Materials Science and Engineering, McMaster University.

Ollson, R. G. (1965). "Rate of dissolution of carbon-steel in molten iron-carbon alloys." Ibid., 233: 1654.

Ostman, M. (2006). Melting Pre-Study of Models and Mapping- Physical Modelling of Scrap Melting (Master's Thesis). Department of Applied Physics and Mechanical Engineering, Lulea University of Technology, Lulea, Sweden.

Pehlke, R. D., Goodell, P. D., Dunlap, R. W. (1965). "Kinetics of steel dissolution in molten pig iron." Transactions of the Metallurgical Society of AIME, 233; 1420-1427.

Rudzki, E. M., Reinbold, R. J. and Pease, B. K. (1972). Electric Furnace Conference Proceedings, Vol 30, 186-191.

Rudzki, E. M., Reinbold, R. J. and Pease, B. K. (1973). Journal of Metals, 38-44.

Shifrin, V., Popenov, L., Devaux, M. (2001). Steel Times, 281-282.

Sides, P.J. (2002). "Scaling of Differential Equations : Analysis of the Fourth Kind." Chemical Engineering Education, 4681-4698.

http://www.steel.org. Retrieved Aug. 3, 2010, American Steel and Iron Institute, Washington D. C., USA.

Steel University: Electric Arc Furnace. Retrieved Aug. 4, 2010 from http://www.steeluniversity.org/content/html/eng/default.asp?catid=25&pageid=208127193. International Iron and Steel Institute and MATTER, University of

Liverpool, UK.

Szekely, J., Themelis, N. J. (1971). Rate Phenomena in Process Metallurgy. NY, USA, Wiley & Sons Press.

Szekely, J., Chuang, Y. K., Hlinka, J. W. (1972). "The modeling and dissolution of low carbon steels in iron-carbon melts." Metallurgical Transactions, 3(12): 2825-283.

Tang, X., Kirschen, M., Abel, M., Pfeifer, H. (2003), Steel Research, Vol 74, No 3, 201-210.

Schematic diagram of an AC Electric Arc Furnace. Retrieved Oct. 10, 2010 from http://www.teara.govt.nz/en/iron-and-steel/2/4. The Encyclopedia of New Zealand, Wellington, New Zealand.

Teoh, L. L. (1989). Ironmaking & Steelmaking, Vol 16, 303-313.

http://www.thecanadianencyclopedia.com Retrieved Aug. 3, 2010, The Historica Dominion Institute, Toronto, ON.

Thomson, M. J., Kournetas, N. G., Evenson, E., Sommerville, I. D., Guerard, J. (2001). Ironmaking & Steelmaking, Vol 28, No 3, 266-272.

Wells, M. B., Vonesh, F. A. (1986). Iron & Steelmaker, 13-22.

Wright, J. K. (1989). "Steel diffusion in quiescent and gas stirred Fe/C melts." Metallurgical Transactions B, 20B; 363-374.